MARMARA UNIVERSITY

FACULTY OF ENGEENIRING

DEVELOPMENT OF A PARALLEL ORIENTATION MECHANISM IN ROBOTICS

SELEN VARİŞ – 150416008

ME4098 Engineering Project II

Final Report

Supervisor

Asst. Prof. Uğur TÜMERDEM

ISTANBUL, 2022

MARMARA UNIVERSITY

FACULTY OF ENGEENIRING

Development of a Parallel Orientation Mechanism in Robotics

by

Selen Variş, February, 2022

SUBMITTED TO THE DEPARTMENT OF MECHANICAL ENGINEERING I N PARTIAL FULFILLMENT OF THE REQUIREMENTS FOR THE DEGREE

OF

BACHELOR OF SCIENCE

AT

MARMARA UNIVERSITY

Signature of Author(s) .....

Department of Mechanical Engineering

Certified By .....

Project Supervisor, Department of Mechanical Engineering

Accepted By.....

Head of the Department of Mechanical Engineering

ACKNOWLEDGEMENT

First of all, I would like to thank and grateful my supervisor, Asst. Prof. Dr. Uğur Tümerdem for guiding me with his valuable information, for his patience during my study, and for sharing all his resources so that I could be successful and learn in this study.

February, 2022 Selen Variş

CONTENTS

ABSTRACT

Development of a Parallel Orientation Mechanism in Robotics

Parallel orientational mechanisms or in other words wrist mechanisms are widely used in surgeries, especially recently. Also, these mechanisms used in space program (according to NATO space program is still part of military applications) as a platform for observation of planets, stars, and galaxies. Parallel orientation mechanisms also actively used in robotics as security cameras, drones, and military radar systems for communication. Usage types of this mechanism are generally 3 DOF parallel orientational mechanism or 4 DOF parallel orientational mechanism. Generally, singularity problems occurred in 3 DOF parallel orientational mechanisms. Also, we encountered wrist mechanics with 3 DOF but the problem with these mechanisms was that the range of motion were too narrow.

In this thesis, a parallel orientational mechanism is presented with 3 degree of freedoms. This mechanism consists of three revolute joints that a moving platform to a fixed base. This mechanism has two interconnected universal joints extending from the middle of the fixed base to the middle of the mobile ceiling and has 3 revolute motors, all of them are located on intersection point of the limbs with the fixed base. The universal joints will make the rotation movement with the screw movement, through the channels opened between them and the upper platform. The original 3D design of this mechanism was done using SolidWorks.

My purpose in this thesis study, produce a feasible and can be controlled mechanism that got rid of all the problems mentioned above by creating a parallel orientation mechanism with 3 DOFs with 3 motors and 240 degrees range of motion. Thus, an economical solution will be produced by using less motors and creating more movement area.

The kinematic analysis of the designed parallel orientation mechanism was made. A kinematic model of the mechanism was created using kinematic equations. Then it was checked whether it was fit for purpose or not using Matlab/Simulink. Then, by obtaining

the dynamic model of the system in the simulation environment, the position controller has been developed and the feasibility of the system has been demonstrated.

SYMBOLS

Symbol	Quantity	Unit
α	: Pitch angle	deg
β	: Yaw angle	deg
Υ	: Screw angle	deg
θ_i (i=1,2,3)	: Link angles	deg
r	: Radial distance	mm
$\hat{n}_P$	: Orientation vector	
M_i (i=1,2,3)	: Midplane points	
K_i (i=1,2,3)	: Fixed points of the bottom platform	
s_i (i=1,2,3)	: sine	
c_i (i=1,2,3)	: cosine	
$\hat{n}_B$	: Base platform unit vector	
P	: Center point of the top platform	
${}^B_P T$	: Transformation matrix from base to top platform	
r_0	: Initial thrust distance	mm
Δr	: Displacement in thrust axis	mm
φ	: Total orientation angle (pitch and yaw)	deg
φ_1	: Center leg bending angle 1	deg
φ_2	: Center leg bending angle 2	deg
l_i (i=1,2,3)	: Lenght parameters of center leg	mm
Δd	: Displacement of the screw motion	mm
h	: Displacement of the screw motion	mm
p	: Pitch of screw	mm

N_t	: Number of turns	
${}^{0}_{4}T$	: Transformation matrix from {0} to{4}	
${}^{0}_{4}R$	: Rotation matrix from {0} to {4}	
${}^{0}P_{4j}$ (j=x,y,z)	:The position vector with respect to base frame	
R_d	: Desired rotation matrix	
ϕ, Ψ, ϑ	: Euler angles	deg
J_w	: Jacobian between θ_i and $\hat{n}_P$-r	
J_T	: Jacobian between $\hat{n}_P$-r and $\alpha - \beta$	
$J_{\Delta d}$	: Jacobian between r and Δd	
J_Υ	: Jacobian between Δd and Υ	
J	: Total Jacobian of mechanism	

ABREVIATIONS

ALMA **:**Atacam Large Milimeter Array

DOF **:**Degree of Freedom

ESO **:**European Organization for Astronomical Research in the Southern Hemisphere

FANUC **:**Factory Automation Numerical Control

HP1 **:**Heterochromatin Protein 1

MATLAB **:**Matrix Laboratory

MMT **:**Multiple Mirror Telescope

NATO **:**North Atlantic Treaty Organization

POM **:**Parallel Orientation Mechanism

PRR **:**Prismatic-Revolute-Revolute

PU **:**Prismatic- Universal

RRR **:**Revolute-Revolute-Revolute

RSR **:**Revolute-Spherical-Revolute

SGR **:**Security Guard Robot

SPS **:**Spherical- Prismatic- Spherical

3SPS-1S **:**Spherical-Prismatic-Spherical, Spherical

U.S. **:**United States of America

UUP **:**Universal-Universal-Prismatic

VISTA **:**Visible and Infrared Survey Telescope for Astronomy

DH :Denavit-Hartenberg

LIST OF FIGURES

LIST OF TABLES

1. INTRODUCTION

Parallel mechanisms can be defined as closed loop mechanisms that have at least two independent kinematic chains. Parallel mechanisms have an end-effector with n DOF and a fixed base with links. Movement is provided by n simple actuators (1). Parallel mechanisms are commonly claimed to offer several advantages, like high structural rigidity, high speed, high accuracy, heavy payload carriage, fixed actuators. The potential applications of parallel manipulators include mining machines, walking machines, both terrestrial and space applications including areas. For example, in February 1999 an eight-legged parallel robot was used to isolate the space shuttle load from vibration. In addition, medical fields, haptic devices, vehicle suspensions, cable-actuated cameras parallel mechanisms are frequently used. Almost all land-based telescopes make use of parallel mechanisms. For example, the University of Arizona MMT or the European Organisation for Astronomical Research in the Southern Hemisphere (ESO) Visible and Infrared Survey Telescope for Astronomy (VISTA) (1) (2). There are disadvantages as well as such various usage areas and advantages. It offers small and limited workspace due to the interference of the links. In addition, universal and spherical joints cause physical restrictions. Actuators range of motion suffers from the singularities problem (2).

Scientists have taken an interest in parallel robotics with less than six degrees of freedom. Because there is no need for applications to be able to move and rotate. Also, if using less than 6 DOF manipulators decreases the costs. The called parallel wrist mechanisms are 3 DOF spherical manipulators using three revolute joints to orient things. It is divided into over constrained and non-over constrained. It is easier to divide non-over constrained parallel wrists into two:

The first category consists of mechanisms that are just mechanisms that geometric conditions are spherical motions. The second category consists of mechanism exist the base and the platform linked by spherical joint. These mechanisms rotate around it. Mechanisms in the first category must avoid singular configuration throughout their motion. Because it can lose spherical motion and translation movements.

Mechanisms in the second category do not allow the platform to translate. This means more error tolerances. But the second category of manipulators are cheaper. In addition, robots in this group have smaller workspaces (3). The most famous example of parallel mechanisms is the Gough-Stewart platform. The simple principles of the mechanism were established by V.E. Gough in 1947. That structure allows the positioning and orientation of a moving platform to test tire wear and tear.

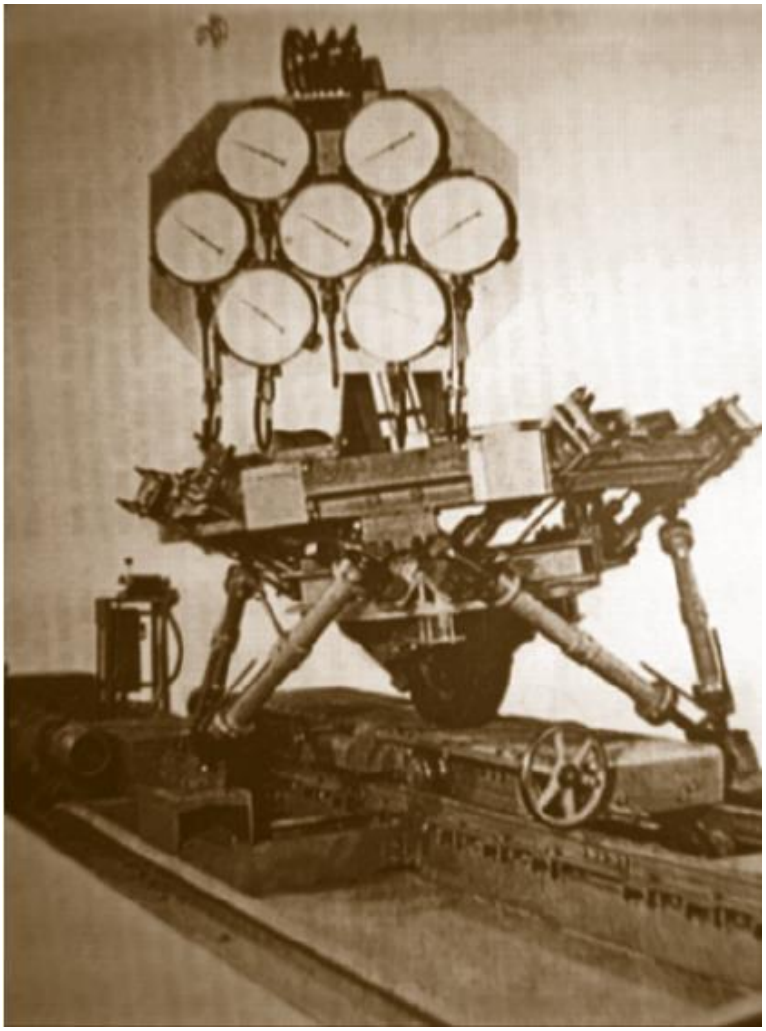

Figure 1.1. Gough Platform, the moving platform to which a tire is attached by a conveyor belt and driven by it. (1947) (1)

In 1955, a prototype was built. This construction consists of a fixed hexagonal platform and a moving top platform. These two platforms are connected with 6 links using ball and socket (spherical) joints. Linear actuator changes the total length of link, so this mechanism works with 6 linear actuators. It has 6 DOF. This 6 DOF is divided into 3 coordinate positioning and 3 orientating angles the first to create and build the famous octahedral hexapod was Gough. Klaus Cappel later developed the very same hexapod independently, patented it and sold it to the first flight simulator firms (4).

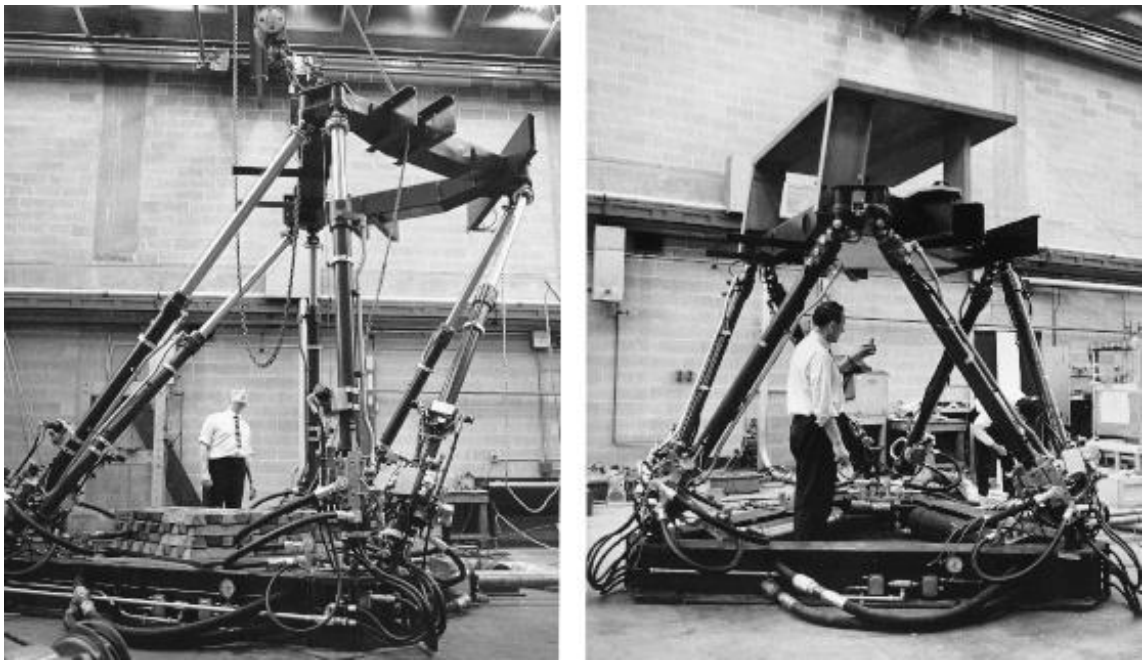

Figure 1.2. A flight simulator designed by Klaus Cappel in the 1960s

While some sources refer to it as the Gough platform, it is often referred to as the Gough-Stewart platform. There are resources, which are also called Hexapod platforms. Stewart's name was added to this architecture since in reviewers remarks on a paper published by Stewart in 1965, Gough's earlier work and a photograph of this platform were mentioned. (4) Stewart revised the same mechanism on the triangle bottom platform. In addition, by adding a universal joint to the links, it made the vertical axis link turn around itself. Gough-Stewart platforms are still preferred for flight simulators today (5) (6).

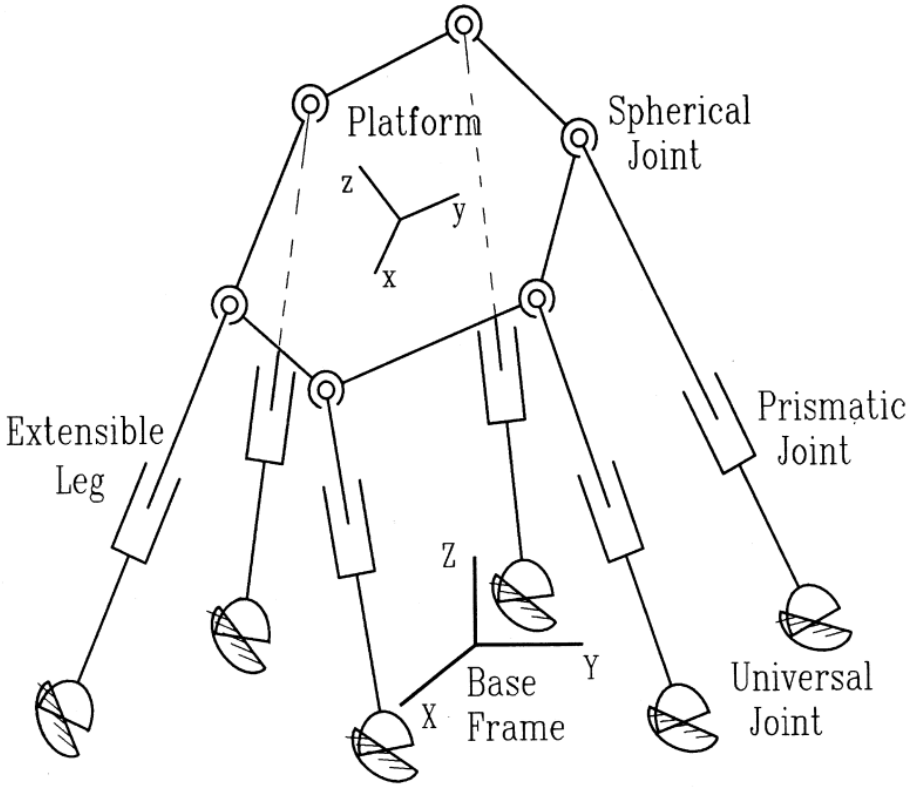

Figure 1.3. The Stewart Platform (7)

Although these structures are still used today, forward kinematic analysis equations complicate them. This problem is the biggest obstacle to the derivation of dynamic equations. This is necessary for developing some sort of model which is necessary for industrial application of the manipulator. Efforts were made to find effective solutions. But the results are not rousing (8).

Apart from the Gough-Stewart platform, another famous parallel robot is the Delta robot. The Delta robot was invented by Reymond Clavel in the 1980s. During a visit to a chocolate factory, it was thought that it would be unhygienic for workers to do everything manually, and a robot was wanted to be developed. The main goal in the development of this robot was to manipulate small objects at higher speed. The companies take advantage of the Delta robot's high speed are the packaging, medical and pharmaceutical industries (4).

Figure 1.4. A FANUC branded Delta robot (https://conceptsystemsinc.com/delta-robots-in-the-food-industry/)

Figure 1.5. The SurgiScope by Intellegent surgical ınstruments&systems (Medical application of the Delta robot)

It is formed over the base plate that does not move as shown in the Figure 1.6. For 4 DOF, 4 motors are needed. There are three kinematic chain links connecting the base plate and the moving plate. Each of these chains consists of an arm and a forearm, and the forearms consist of two parallel links. The reason for using two parallel rods is to avoid the use of universal joints. The forearm links and the moving plate are combined using a spherical joint (9).

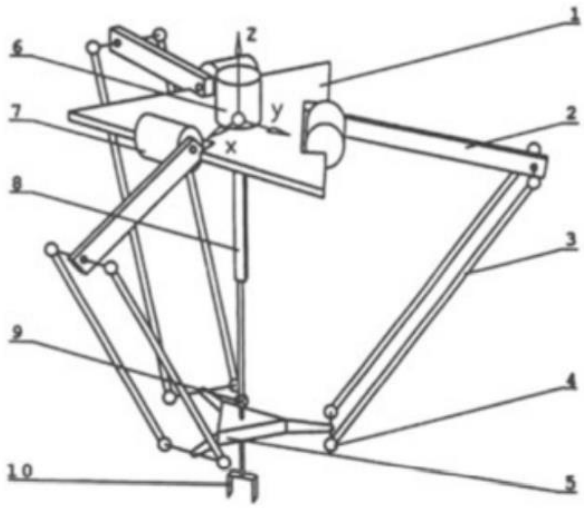

1	Base plate
2	Arm
3	Forearm
4	Spherical joint
5	Travelling plate
6	Actuator of axis # 4
7	Actuator (axis 1- 3)
8	Telescopic transmission
9	Universal joint
10	Gripper

Figure 1.6. The angular Delta Robot (9)

The main problem of Delta robots is small work spacing, as in all parallel mechanisms. Also, this mechanism was disability to operate with heavy objects. That is why it is used in micro fabrication applications. Delta robots are widely chosen as a micro factory manipulation mechanism (10).

Another example is the Tricept parallel manipulator. K-E. It was introduced by Neumann. It consists of a fixed base and a mobile upper platform. 3 arms connect these two platforms. Each arm consists of spherical-prismatic-spherical (SPS) kinematic chain. It has 3 DOFs, two rotational and one translation. Also, as shown in the Figure 1.7, a universal joint can be connected instead of a spherical joint. When the Prismatic-universal (PU) has kinematic character, the moving platform also has 3 DOF (11).

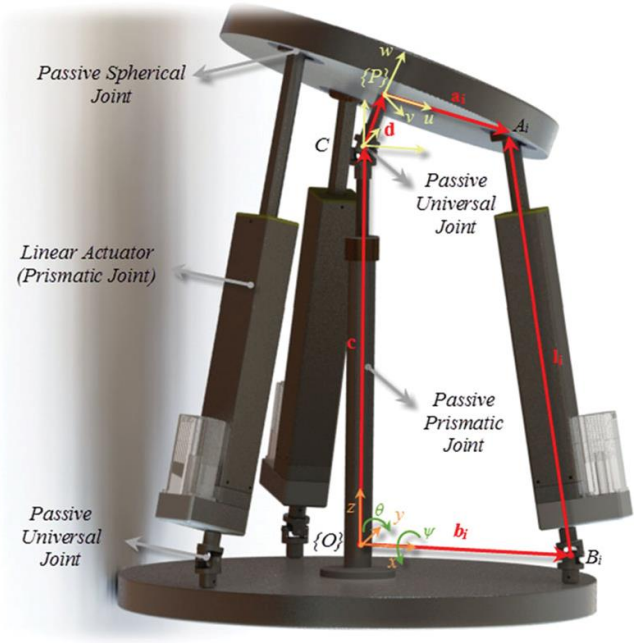

Figure 1.7. Tricept Manipulator (11)

This robot used industrially is generally used in the automobile industry. Other applications are deburring, milling, woodworking, laser and water jet cutting, spotting and laser welding (11) (12).

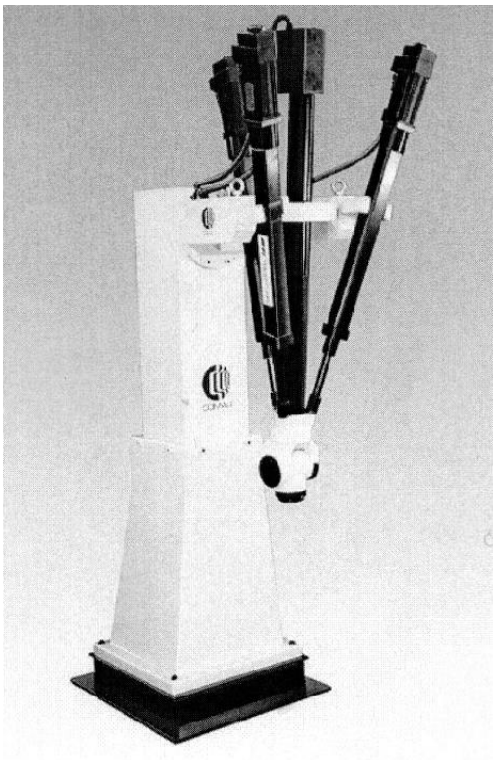

Figure 1.8. The robot Comau Tricept HP1

The orientation mechanisms have been used in security and defense applications. Examples include Samsung Techwin's SGR series of surveillance robots and sentry weapons. Sentry weapons (defense systems) must have very high precision, in order to meet their targets accurately, and load power, so that when firing, and it does not turn (13).

(a) **(b)**

Figure 1.9. a) Parallel robot used as sentry device b) Parallel robot as a surveillance system (14).

Figure 1.10. Samsung SGR-1 Tracking and Surveillance Robot

Another is the parallel manipulator developed by Cui and Zhang, which prevents unnecessary movements by simply performing rotational movements. This mechanism consists of the 3SPS-1S central leg (Figure 6). This parallel mechanism has more accuracy. It is a good candidate for use in security and defense applications (3).

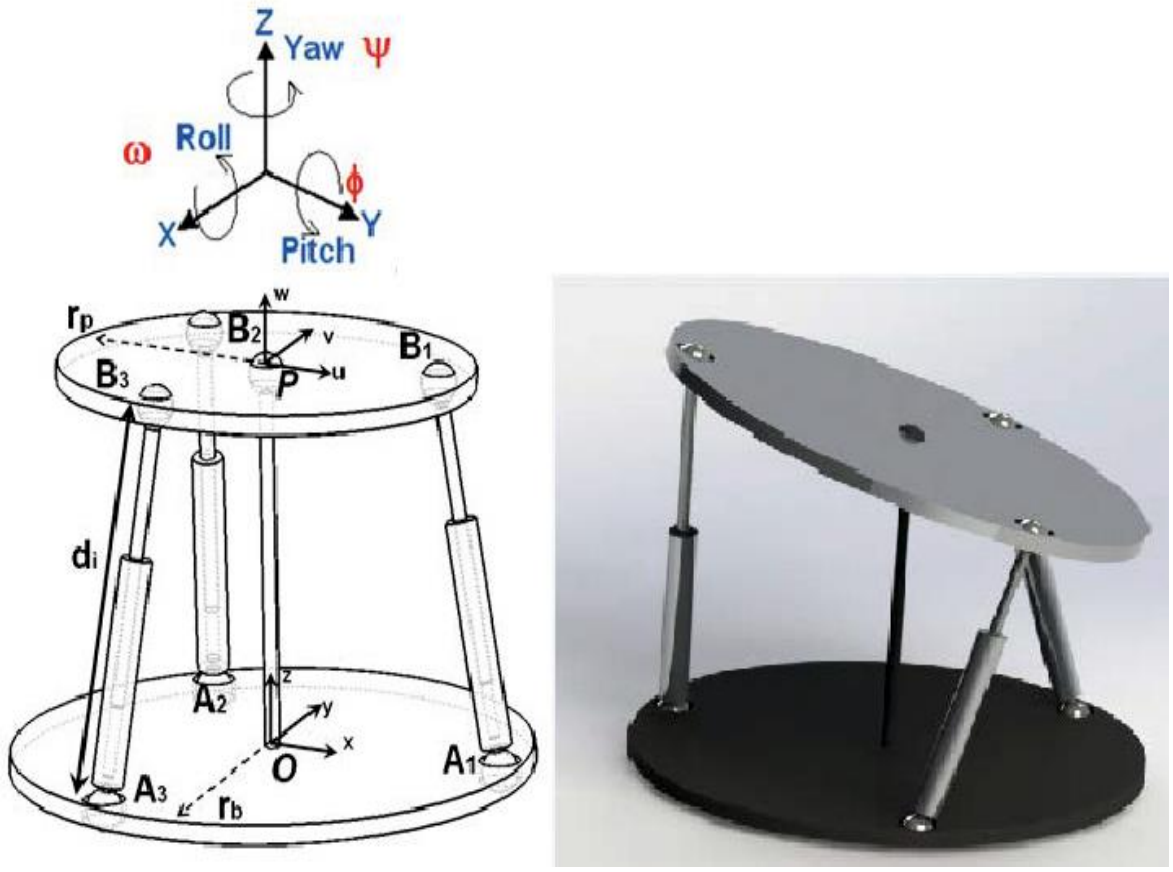

Figure 1.11. Model of the 3SPS-1S parallel wrist

Parallel mechanisms also have applications in orienting the satellite antennas and telescopes. Canterburry satellite viewer uses parallel mechanism for better orientation. The robot consists of two parts. 3 DOF prismatic joint with fixed length for slide and 3 DOF revolute joint for swing. The model encourages emergency activity to contribute to emergency behaviour. Saving costs building, launching, and operating in space applications (2).

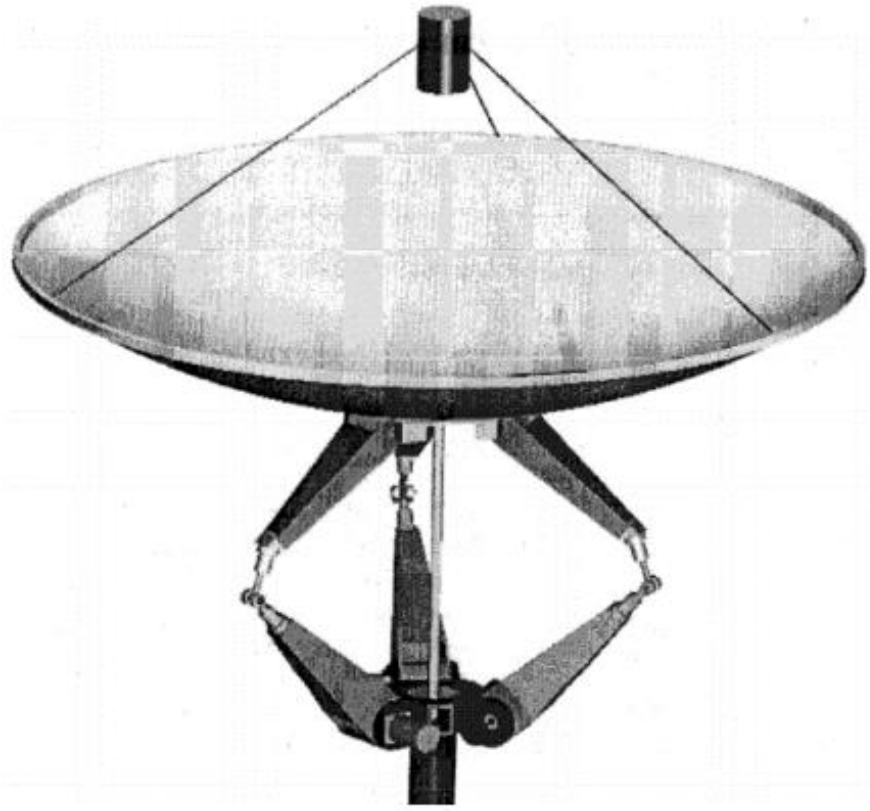

Figure 1.12. Canterburry Satellite Tracker (2).

Especially Stewart platform is widely used for telescopes. LMT (Large Millimeter Telescope), Effelsberg, ALMA (Atacama Large Millimeter Array), NSRT (The NanShan Radio Telescope) these are examples of radio telescopes (15).

(a) **(b)**

Figure 1.13. a) LMT (Large Millimeter Telescope) b) ALMA (Atacama Large Millimeter Array)

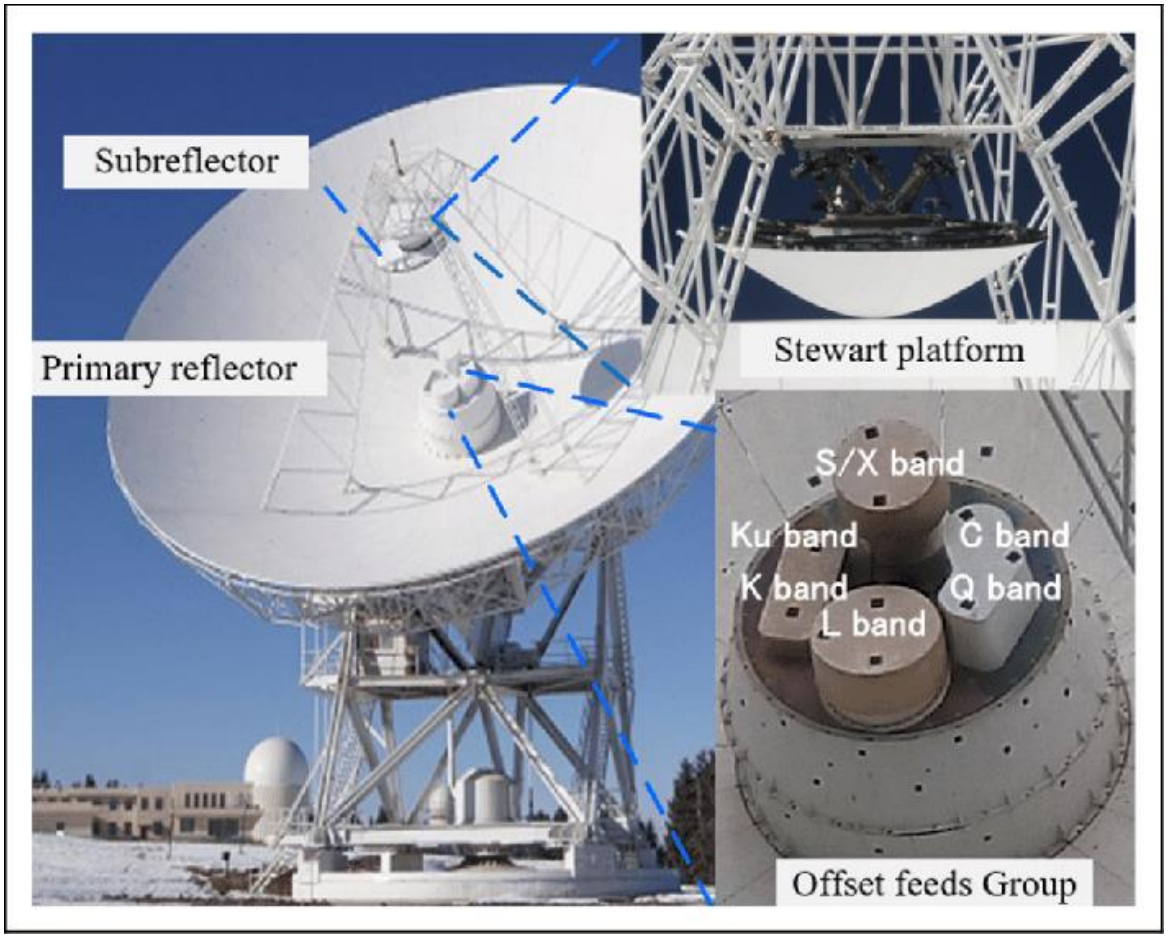

Figure 1.14. The NSRT (NanShan Radio Telescope) (15)

As an example of orientation mechanisms, we can give the example of camera-orienting device Agile Eye. It was introduced by Laval University in the 1990s (16) and a prototype was produced. It was built by Tianjin University. With 3 RRR kinematic chains, this device could mark a 140 degree (±30 degree torsion) cone. This spherical orientation parallel mechanism has 3 DOFs. Unfortunately, Agile Eye has the same problems with other parallel mechanisms. the singularities of the six curves in the three-dimensional workspace are the Agile Eye, corresponding to self-motions and settings for lockups. These problems are still identified and kinematic solutions are still produced (17).

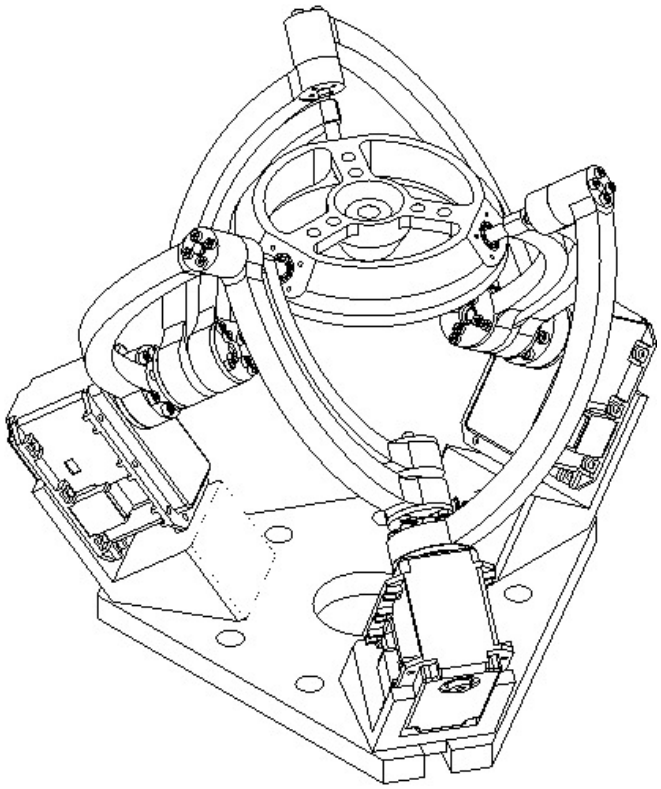

Figure 1.15. The Agile Eye design

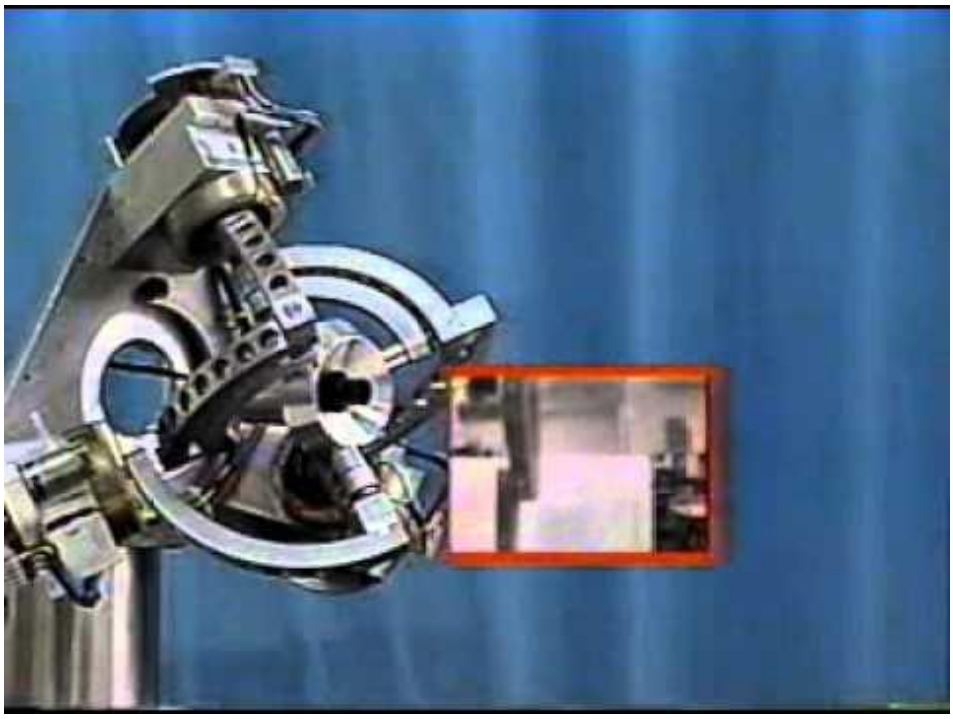

Figure 1.16. The Agile Eye by Laval University

Omri-Wrist III is an orientation mechanism developed in the U.S. This mechanism developed by Ross-Hime has been named as tracking and marking mechanism in laser communication system (18). It has 2 DOFs and works with two linear motors. It is capable of a full ±90 hemisphere movements. This mechanism offers features such as easy to manufacture, cheapness, high rotation rates, high accuracy and singularity-free. Stabilized platforms are widely used in areas such as monitoring devices (19).

Figure 1.17. Omni-Wrist III

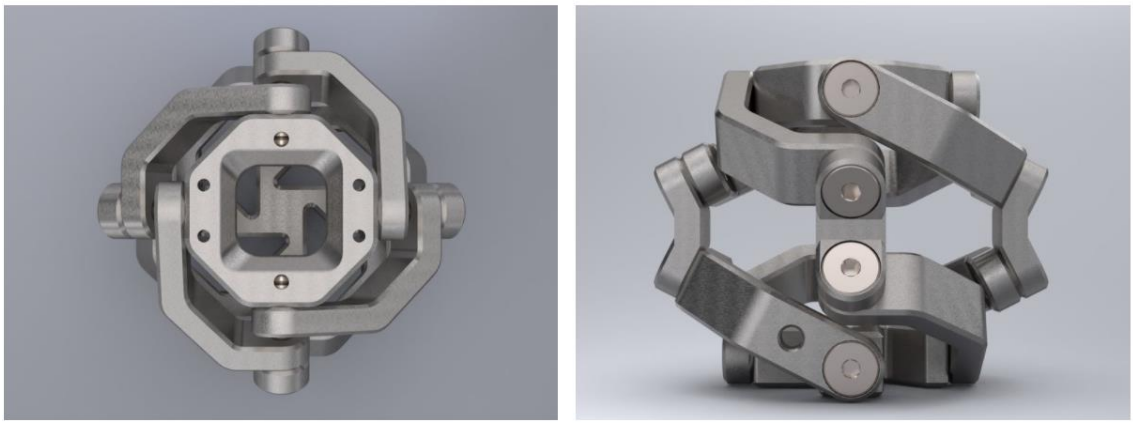

Figure 1.18. Omni-Wrist III (http://www.soheil-sadeqi.com/parallelmanip#orientation-manipulator)

2. MECHANICAL DESIGN OF A PARALLEL ORIENTATION MECHANISM

The parallel orientation mechanism can imitate the motion of pronation/supination with roll movement. Since it can easily perform the movements of the wrist mechanism, it can be used in various functions in space, robotics, and communication areas.

In this study, it is aimed to design a parallel orientation mechanism that can be used in various robotic applications, which is economical with 3 motors, and is much more useful than the others with 3DOF and 240-degree axis movement. The design principles, specifications and goals are determined when designing the mechanism, considering the motion capacity of largest areas that can be reached.

First, 3 DOF parallel orientation mechanism has been developed that can only perform tilt and yaw movements. While drawing, the most important thing was to examine and modify previously made POM samples to create a 240-degree movement area as much as possible (20) (21). Also, I want to rotate universal joints by helping screw thread. POMs are very similar to wrist mechanisms, so when I examined the working principles of wrist mechanisms, I saw some main movements; flexion, extension, deviation, pronation, and supination you can see in Figure 2.1. However, my POM can perform these movements smoothly and can perform these movements on the axis of motion that the human wrist and other wrist mechanisms cannot. I create two types of parallel orientation mechanism you can see below in details.

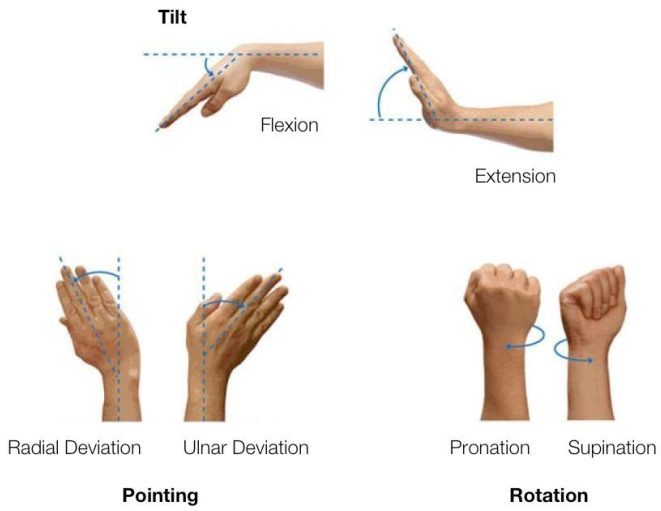

Figure 2.1. DOFs of the human wrist: Flexion, Extension, Deviation, Pronation/Supination.

2.1. Type (1) Parallel Orientation Mechanism

3 revolute motors were designed in the parallel orientation mechanism with 3 DOFs. POM was designed to do all motion types mentioned in Figure 2.1. The mechanism of parallel orientation (wrist) used in these forceps is already presented in (22), (23), (24). The actuation system is composed of revolute motors. The wrist mechanism is controlled by 3 revolute motors. Orientation motions are realized by converting rotate motions via 3-RSR chains.

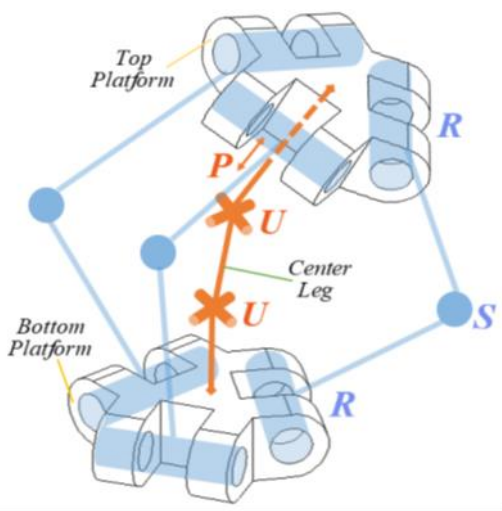

Figure 2.2. The kinematic model of the parallel orientation mechanism RSR and UUP serial chains.

In the tables [Table 2.1. and Table 2.2.], we show our joints and total assembly. Considering the desired motion capacity, the joint types that build up the mechanism are determined. To put it simply, all our connections can rotate (spherical or revolute), and this is logically assembled. 3 identical legs forming the wrist portion of the system are used symmetrically and each connection, which is an aspect of these legs, is linked by revolute joints to each other. A combination of 3 revolute joints perpendicular to each other can be assumed as a spherical joint to simplify the structure.

By combining the mechanism with the screw on universal joint to provide roll motion for the end-effector of the mechanism shown in Table 2.1. as a final assembly. There is a thin and long platform under the mechanism, but since the lower platform is not directly connected to the mechanism, it can be easily placed on different platforms that can be designed according to various usage areas. Even, via the control mechanism, universal

joints can rotate along their own axis. The rolling motion spectrum is ± 360 degrees, so the open working area is extended. Instead of using a linear motor in the mechanism, unnecessary space occupation was avoided thanks to 3 revolute motors and screw threads. Apart from that, by keeping the lower and upper platforms small and keeping the connections between the platforms large and wide, it has been raised up to ±120 degrees.

Revolute Joints			Universal Joints
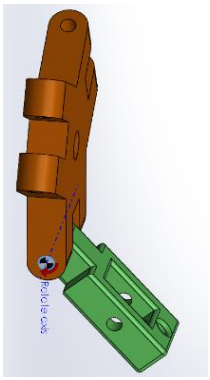	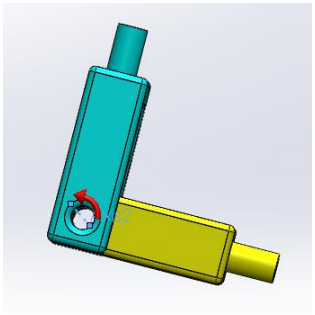	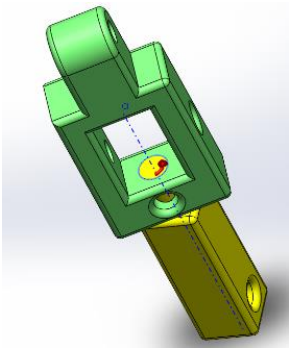	
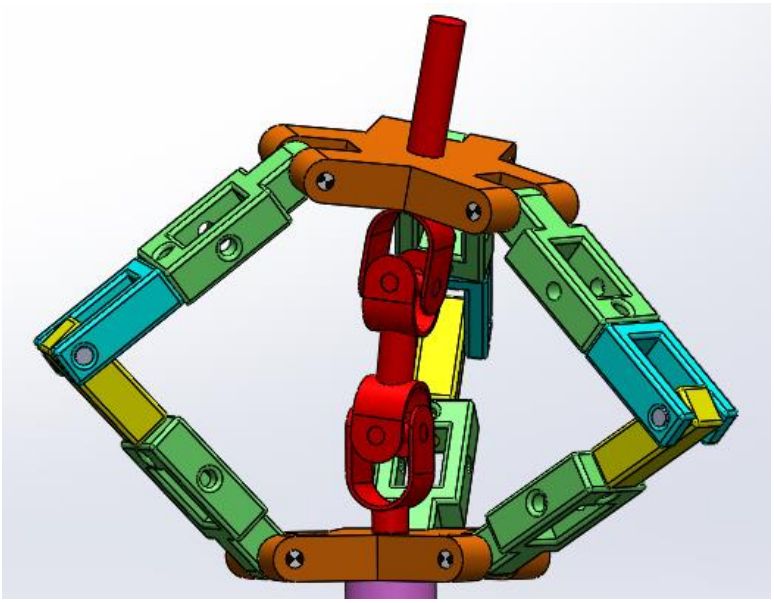			
Final Assembly			

Table 2.1. Revolute Joints, Universal Joints, Final Assembly

Table 2.2. 3-DOF parallel orientation mechanism movement

FLEXION	EXTENSION
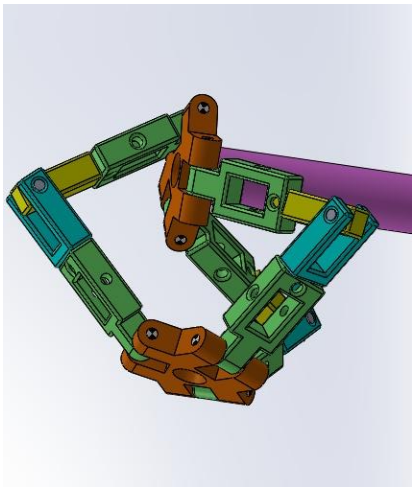	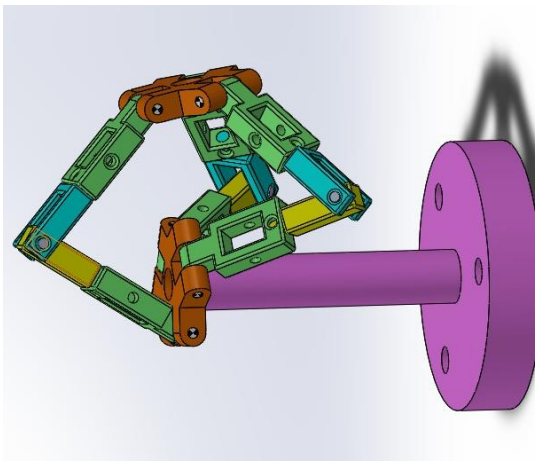
DEVIATION	
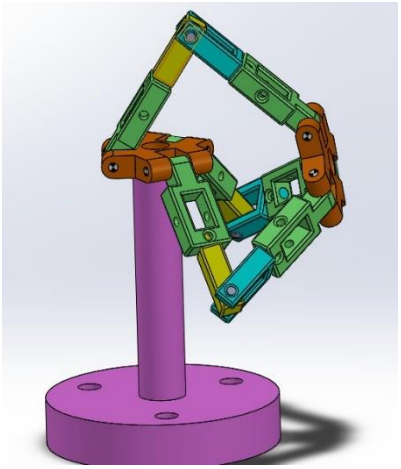	

2.2. Type (2) Parallel Orientation Mechanism

This design is similar to my Type-1 design, but instead of explaining the differences, I wanted to take this design from scratch.

Considering the desired motion capacity, the joint types that build up the mechanism are determined. 3 revolute motors were designed in the parallel orientation mechanism with 3 DOFs. The actuation system is composed of revolute motors and these motors located on bottom platform and it is controlled by 3 revolute motors. This mechanism was designed to do all motion types mentioned in Figure 2.1. It is basically an example for wrist mechanism. The mechanism using 3-RSR (R: Revolute, S: Spherical) serial chains. Orientation motions are realized by converting rotate motions via 3-RSR chains. The mechanism of parallel orientation (wrist) used in these forceps is already presented in (13), (14), (15). Simply put, all my connections are spherical or rotatable and combined with this logic. 3 identical legs forming the wrist portion of the system are used symmetrically and each connection, which is an aspect of these legs, is linked by revolute joints to each other. A combination of 3 revolute joints perpendicular to each other can be assumed as a spherical joint to simplify the structure.

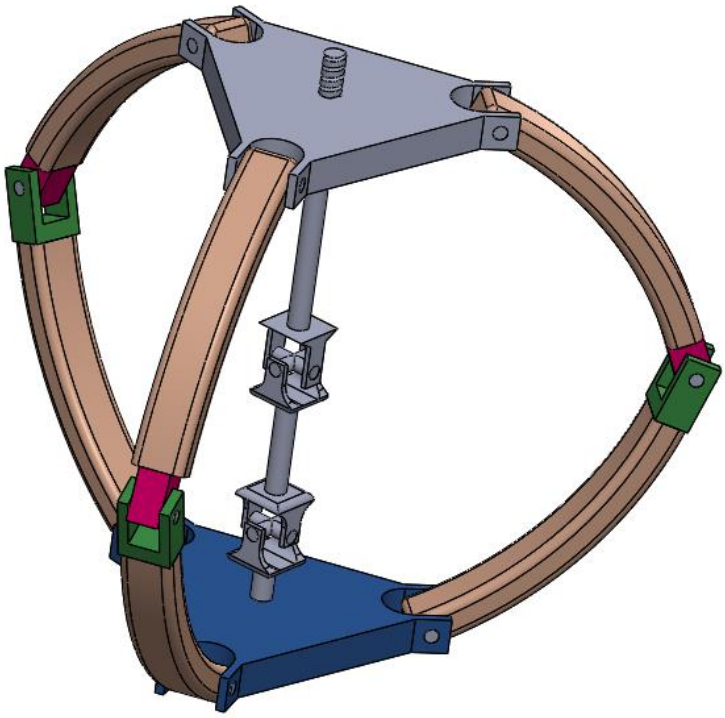

Figure 2.3. Type (2) Parallel orientation mechanism schema

By combining the mechanism with the screw on universal joint to provide roll motion for the end-effector of the mechanism shown in Table 2.3. as a final assembly. In this design, I made the arms extending from the lower platform to the upper platform in a curve, and I also made the lower and upper platform smaller and tried to make the general structure of my design look like a sphere shown in Figure 2.3. The rolling motion spectrum is ± 360 degrees, so the open working area is extended. The main purpose of this design was to reach a width of ±120 degrees.

Table 2.3. Revolute Joints, Universal Joints, Final Assembly

Revolute Joints			
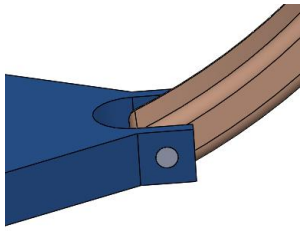	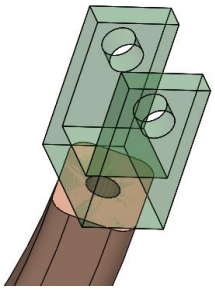	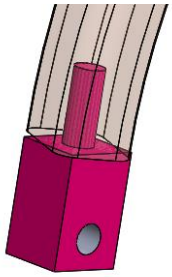	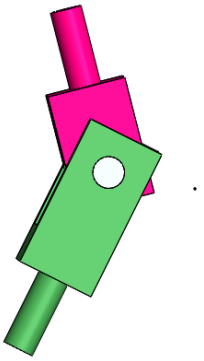

Universal Joints	
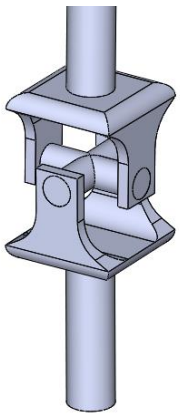	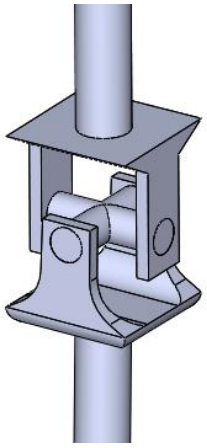

Final Assembly
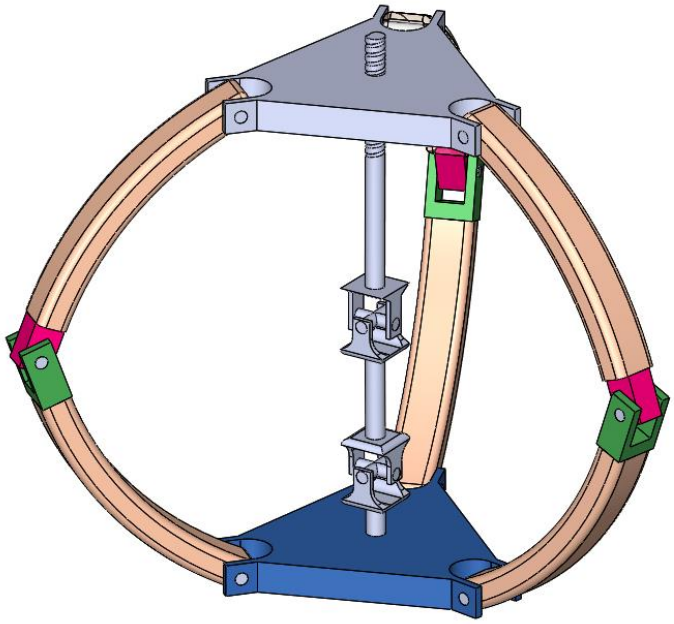

Table 2.4. 3-DOF parallel orientation mechanism movement

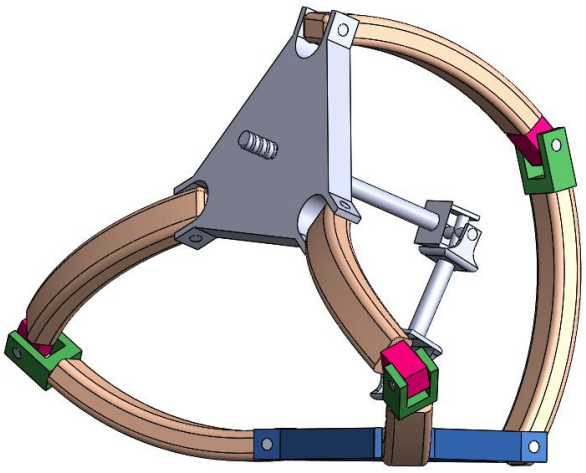	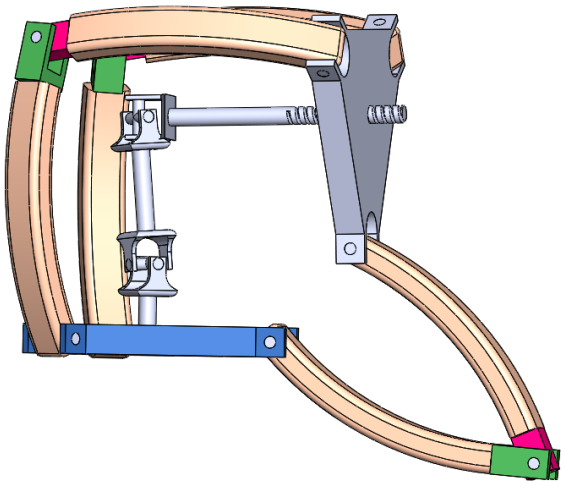

3. KINEMATICS ANALYSIS

In this section, kinematic analysis of the parallel orientation mechanism is made. It has been examined under two headings as position kinematic analysis and velocity kinematic analysis.

3.1. Position Kinematic Analysis

In this section, the forward and inverse kinematic equations of the parallel orientation mechanism are found using geometrical constraints. Figure 3.1 shows a general scheme of forward and inverse kinematics. It shows how pitch (α), yaw (β) and screw angle (Υ)are found based on motor angles (θ_i), and vice versa.

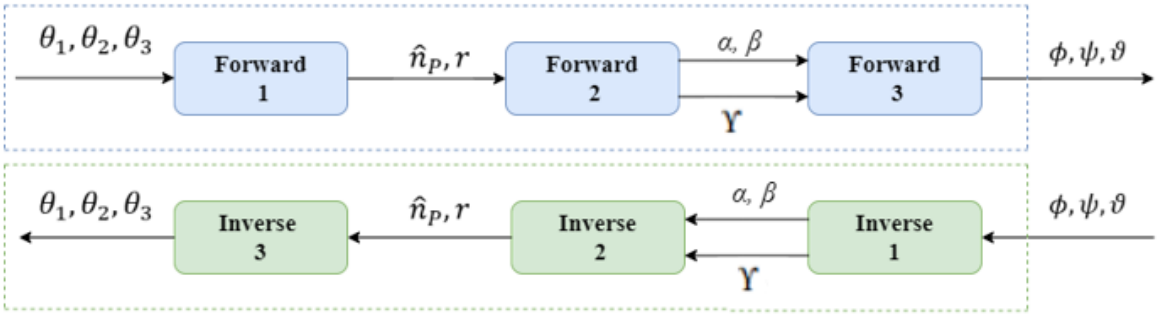

Figure 3.1 Position kinematic analysis steps

3.1.1. Forward Kinematics

Forward kinematic analysis for the parallel orientation mechanism gives pitch (α), yaw (β) and screw angle (Υ). Angles of rotary motors (θ_i) are used as input value.

a. Forward 1

In this section, unit vector of the tool orientation ($\hat{n}_P$) and radial distance (r) are calculated based on link angles (θ_i). ${}^{B}M_i$ is a midplane point that can be calculated by adding ${}^{B}K_i$, a fixed point on the wrist's bottom platform, and vector $F_i^B t_i$, as shown in Figure 3.2.

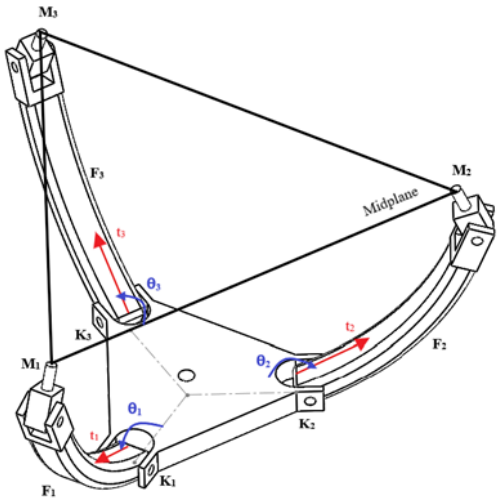

Figure 3.2 Visualization of kinematic structure including vectors and points on the wrist part

$$^{B}M_i = {}^{B}K_i + F_i{}^{B}t_i \tag{3.1}$$

where F_i is a constant link length, ${}^{B}t_i$ is an unit vector of $F_i{}^{B}t_i$.

$$^{B}t_i = \begin{bmatrix} s_i \\ -c_i c_{\Phi_i} \\ -c_i s_{\Phi_i} \end{bmatrix} \tag{3.2}$$

In Φ_i is 180º, 300º and 60º respectively with $s_i = \sin(\theta_i)$ and $c_i = \cos(\theta_i)$ where $i = 1{:}\,3$.

$$^{B}t_1 = \begin{bmatrix} s_1 \\ c_1 \\ 0 \end{bmatrix}, \qquad ^{B}t_2 = \begin{bmatrix} s_2 \\ -\frac{1}{2}c_2 \\ \frac{\sqrt{3}}{2}c_2 \end{bmatrix}, \qquad ^{B}t_3 = \begin{bmatrix} s_3 \\ -\frac{1}{2}c_3 \\ -\frac{\sqrt{3}}{2}c_3 \end{bmatrix} \tag{3.3}$$

The unit vector projecting from the bottom platform's origin to the top platform's origin is found.

$$\hat{u} = \begin{bmatrix} \hat{u}_x \\ \hat{u}_y \\ \hat{u}_z \end{bmatrix} = \frac{({}^{B}M_2 - {}^{B}M_1) \cdot ({}^{B}M_3 - {}^{B}M_1)}{|({}^{B}M_2 - {}^{B}M_1) \cdot ({}^{B}M_3 - {}^{B}M_1)|} \tag{3.4}$$

where ${}^{B}M_i$ and ${}^{B}K_i$ are defined based on Figure 3.2

$$ {}^{B}M_1 = \begin{bmatrix} Fs_1 \\ K_{1y} + Fc_1 \\ 0 \end{bmatrix}, \; {}^{B}M_2 = \begin{bmatrix} Fs_2 \\ K_{2y} - \frac{F}{2}c_2 \\ K_{2z} + \frac{\sqrt{3}F}{2}c_2 \end{bmatrix}, \; {}^{B}M_3 = \begin{bmatrix} Fs_3 \\ K_{3y} - \frac{F}{2}c_3 \\ K_{3z} - \frac{\sqrt{3}F}{2}c_3 \end{bmatrix} \tag{3.5} $$

$$ {}^{B}K_1 = \begin{bmatrix} 0 \\ \frac{-L_0}{2\sqrt{3}} \\ 0 \end{bmatrix}, \qquad {}^{B}K_2 = \begin{bmatrix} 0 \\ \frac{L_0}{4\sqrt{3}} \\ \frac{-L_0}{4} \end{bmatrix}, \qquad {}^{B}K_3 = \begin{bmatrix} 0 \\ \frac{L_0}{4\sqrt{3}} \\ \frac{L_0}{4} \end{bmatrix} \tag{3.6} $$

The thrust distance *r* is calculated using the relation that *P/2* is the projection of *r* onto the unit vector $\hat{u}$, as shown in Figure 3.4.

$$ r = \frac{P}{2\hat{n}_B \cdot \hat{u}} \tag{3.7} $$

and

$$ P = 2({}^{B}M_1 \cdot \hat{u}) \tag{3.8} $$

where $\hat{n}_B$ is the unit vector perpendicular to the center of the bottom platform

$\hat{n}_B = [1 \quad 0 \quad 0]^T$ and P is the distance between the center points of the top and bottom platforms projection of the point which can be computed using the relation that P is the projection of any vertices on midplane ${}^{B}M_1$ onto $\hat{u}$.

$$ r = \frac{P}{2\hat{u}_x} = \frac{{}^{B}M_1 \cdot \hat{u}}{\hat{u}_x} \tag{3.9} $$

The tool orientation unit vector $\hat{n}_P$ is found using vector summation:

$$\hat{n}_B r + \hat{n}_P r = {}^B P \tag{3.10}$$

where ${}^B P$:

$${}^B P = \hat{u} P = r \begin{bmatrix} 1 + \hat{n}_{Px} \\ \hat{n}_{Py} \\ \hat{n}_{Pz} \end{bmatrix} \tag{3.11}$$

By substituting (3.7) and (3.8) into (3.10) $\hat{n}_P$ is found;

$$\hat{n}_P = \frac{{}^B P - \hat{n}_B r}{r} = \frac{{}^B P}{r} - \hat{n}_B \tag{3.12}$$

b. Forward 2

In this section is calculated tool bending angles and screw displacement based on unit vector of the tool orientation ($\hat{n}_P$) and radial distance (r). For the purpose of determining α and β, the transformation matrix that expresses orientation and position is derived using modified Denavit-Hartenberg (DH) wrist parameters (Table 3.1). Figure 3.3 shows the frame assignment.

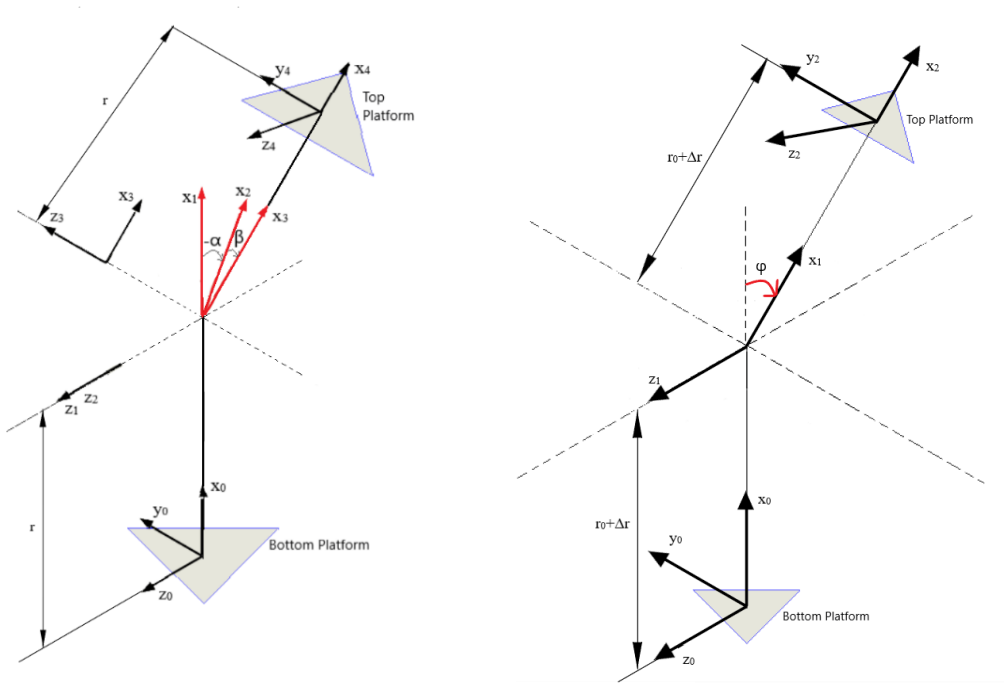

(a) **(b)**

Figure 3.3. The kinematic structure diagrams of the wrist

Table 3.5. DH Parameters of 3 DOF wrist mechanism

i	α_{i-1}	a_{i-1}	d_i	θ_i
1	0	*r*	0	0
2	0	0	0	α
3	$-\pi/2$	0	0	β
4	$\pi/2$	*r*	0	0

$$ {}^{B}_{P}T = \begin{bmatrix} c_\alpha c_\beta & -s_\alpha & c_\alpha s_\beta & r(1+c_\alpha c_\beta) \\ s_\alpha c_\beta & c_\alpha & s_\alpha s_\beta & r s_\alpha c_\beta \\ -s_\beta & 0 & c_\beta & -r s_\beta \\ 0 & 0 & 0 & 1 \end{bmatrix} \tag{3.13} $$

Since the up direction is determined as the x-axis, the first column of the matrix given in is $\hat{n}_P$:

$$\hat{n}_P = \begin{bmatrix} 2\hat{u}_x^2 - 1 \\ 2\hat{u}_x\hat{u}_y \\ 2\hat{u}_x\hat{u}_z \end{bmatrix} = \begin{bmatrix} cos\alpha cos\beta \\ sin\alpha cos\beta \\ -sin\beta \end{bmatrix} = \begin{bmatrix} c_\alpha c_\beta \\ s_\alpha s_\beta \\ -s_\beta \end{bmatrix} \tag{3.14}$$

Thus, α and β can be found,

$$\alpha = atan2(\hat{n}_{Py}, \hat{n}_{Px}) \tag{3.15}$$

$$\beta = atan2\left(-\hat{n}_{Pz}, \sqrt{\hat{n}_{Px}{}^2 + \hat{n}_{Py}{}^2}\right) \tag{3.16}$$

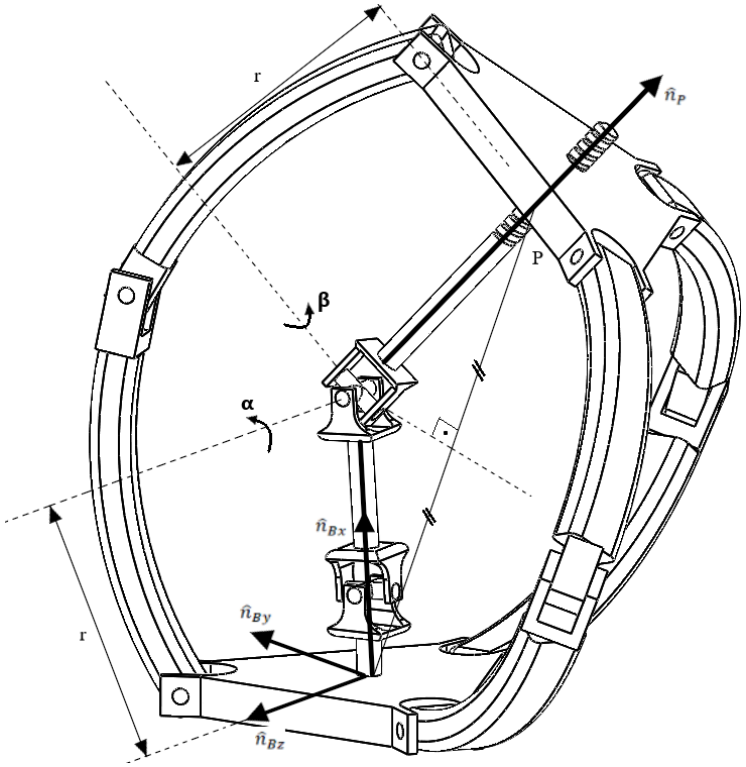

Figure 3.4 Representations of 3 DOF wrist mechanism parameters

$$T_w = \begin{bmatrix} c_\alpha c_\beta & -s_\alpha & c_\alpha s_\beta & (r_0 + \Delta r)(1 + c_\alpha c_\beta) \\ s_\alpha c_\beta & c_\alpha & s_\alpha s_\beta & (r_0 + \Delta r) s_\alpha c_\beta \\ -s_\beta & 0 & c_\beta & -(r_0 + \Delta r) s_\beta \\ 0 & 0 & 0 & 1 \end{bmatrix} \tag{3.17}$$

The sum of the initial thrust distance r_0 and the change in thrust distance Δr is known as r.

$$r = r_0 + \Delta r \tag{3.18}$$

φ, which is found by combining tool orientation angles, is shown in Figure 3.5. It is found with the dot product of the tool unit vector and the unit vector perpendicular to the center of the bottom platform.

$$\varphi = \varphi_1 + \varphi_2 = cos^{-1}\left(\frac{\hat{n}_P \cdot \hat{n}_B}{|\hat{n}_P||\hat{n}_B|}\right) \tag{3.19}$$

Similarly, it is assumed that the center leg moves in two dimensions by translating U joint motions to $\varphi 1$ and $\varphi 2$ as shown in Figure 3.5, and the transformation matrix for the center leg's DH parameters is derived as follows:

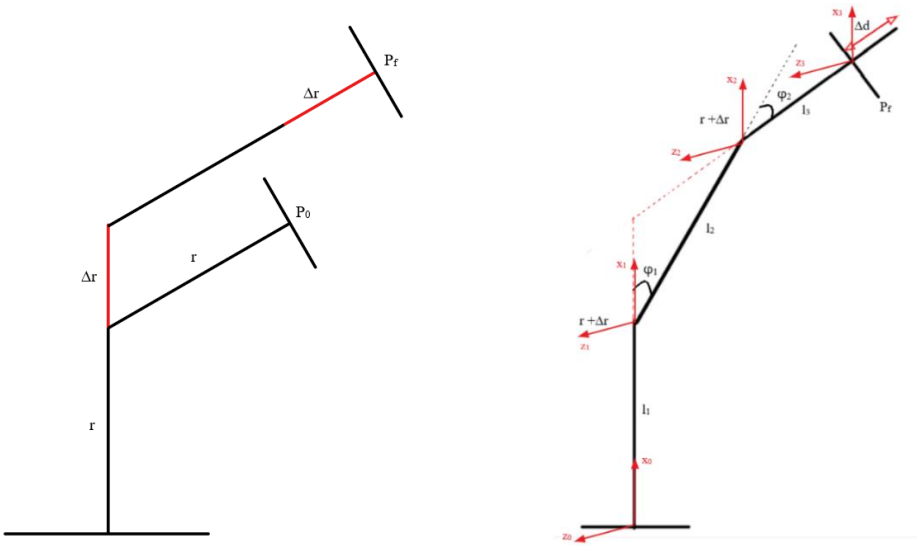

(a) **(b)**

Figure 3.5 Visualization of DH parameters of the center leg

Table 3.6. DH Parameters of the center leg of the wrist mechanism

i	α_{i-1}	a_{i-1}	d_i	θ_i
1	0	l_1	0	φ_1
2	0	l_2	0	φ_2
3	0	$l_3+\Delta d$	0	0

$$ {}^{0}_{3}T = \begin{bmatrix} c\varphi_{12} & -s\varphi_{12} & 0 & l_1 + (l_3 + \Delta d)c\varphi_{12} + l_2 c\varphi_1 \\ s\varphi_{12} & c_\alpha & 0 & (l_3 + \Delta d)s\varphi_{12} + l_2 s\varphi_1 \\ 0 & 0 & 1 & 0 \\ 0 & 0 & 0 & 1 \end{bmatrix} \tag{3.20} $$

By applying the conversion α, β to φ, (3.17) becomes:

$$ T_w{}' = \begin{bmatrix} c_\varphi & -s_\varphi & 0 & (r_0 + \Delta r)(1 + c_\varphi) \\ s_\varphi & c_\varphi & 0 & (r_0 + \Delta r)s_\varphi \\ 0 & 0 & 1 & 0 \\ 0 & 0 & 0 & 1 \end{bmatrix} \tag{3.21} $$

Equate the elements [4,1] and [4,2] in the (3.21) and (3.20) matrices to find Δd.

$$ l_1 + (l_3 + \Delta d)c\varphi_{12} + l_2 c\varphi_1 = (r_0 + \Delta r)(1 + c_\varphi) \tag{3.22} $$

$$ (l_3 + \Delta d)s\varphi_{12} + l_2 s\varphi_1 = (r_0 + \Delta r)s_\varphi \tag{3.23} $$

Thus, Δd that is displacement is found:

$$ \Delta d = l_1 - l_3 - (1 + c_\varphi)\left(l_1 - \mathrm{r} + \sqrt{\frac{{l_2}^2 - (l_1 - r)^2 s_\varphi}{\left(1 + c_\varphi\right)^2}} \right) \tag{3.24} $$

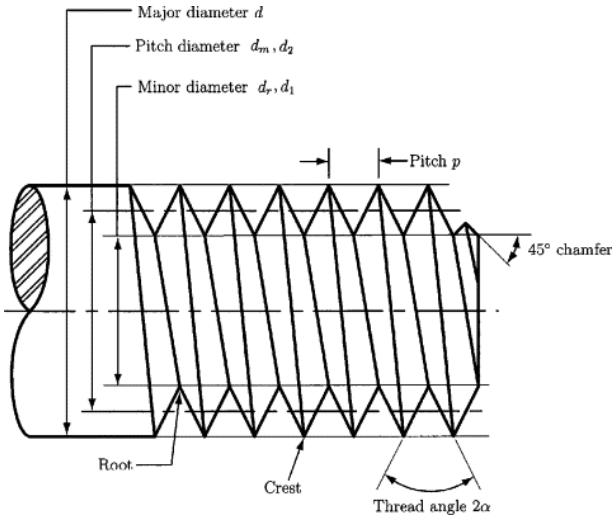

Figure 3.6. End effector screw system details.

In Figure 3.6, we applied the screw type of this mechanism to the inner part of the upper platform with the end effector part. By doing this, we aimed to provide the roll motion without additional motor.

N_t: $Number\ of\ turns$

p: $Pitch\ (distance\ between\ threads)$

h: $displacement$

General formula for screw,

$$h = N_t * p \tag{3.25}$$

So that,

$$N_t = {}^{h}/_{p} \tag{3.26}$$

In our mechanism h is not one way and equal to Δd,

$$h = \Delta d \tag{3.27}$$

If we multiply both sides with 2π,

$$N_t * 2\pi = \left(\Delta d/p\right) * 2\pi \tag{3.28}$$

By multiplying, number of turns and 2π we find the roll angle using Δd and we call screw roll angle as Υ,

$$N_t * 2\pi = \Upsilon \tag{3.29}$$

Finally,

$$\Upsilon = \left(\Delta d/p\right) * 2\pi \tag{3.30}$$

And Δd is found that (3.24);

$$\Upsilon = \left[\frac{l_1 - l_3 - (1 + c_\varphi)\left(l_1 - \mathrm{r} + \sqrt{\frac{{l_2}^2 - (l_1 - r)^2 s_\varphi}{\left(1 + c_\varphi\right)^2}}\right)}{p}\right] * 2\pi \tag{3.31}$$

c. Forward 3

The 3-DOF wrist is modeled as a combination of pitch (α), yaw (β), and roll (γ) in this section. Since there is no motor to provide the roll movement, the roll movement will provide the screw angle (Υ) found in the Forward 2 part.

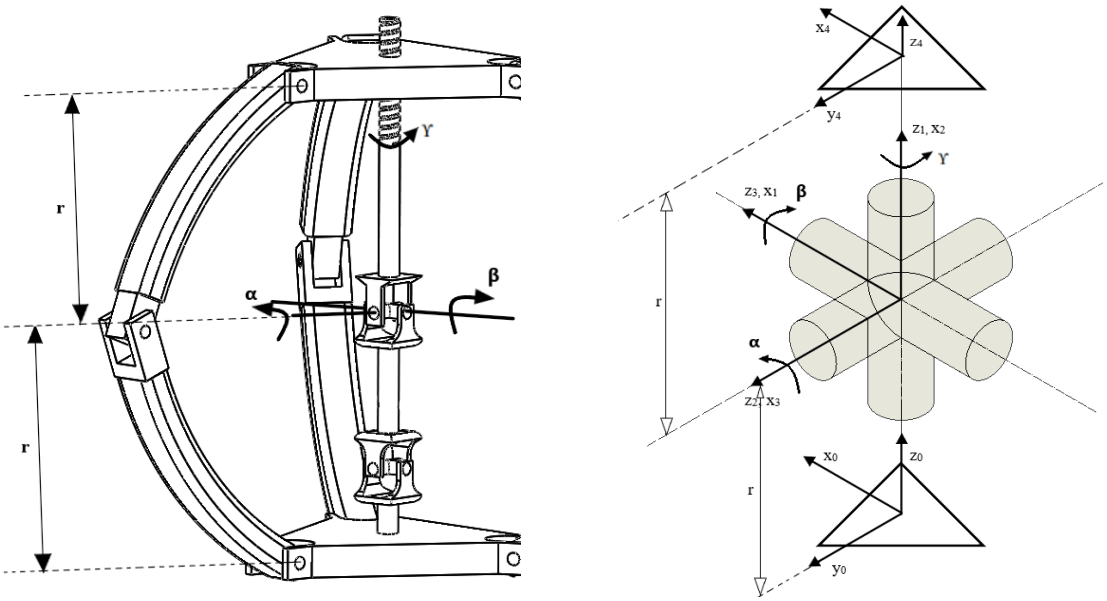

Figure 3.7. Visualization of DH parameters

Table 3.7. DH Parameters of the 3 DOF wrist incluiding roll axis

i	α_{i-1}	a_{i-1}	d_i	θ_i
1	0	0	r	0
2	0	$-\pi/2$	0	$-\pi/2+\alpha$
3	0	$-\pi/2$	0	$-\pi/2+\beta$
4	0	$-\pi/2$	r	$-\pi/2$

The modified DH parameters are described in Table 3.3 based on the frame assignment with respect to the base frame 0 in Figure 3.7. The 3 DOF wrist including roll axis of transformation matrix ${}^{0}_{4}T$, orientation matrix ${}^{0}_{4}R$ and position vector ${}^{0}P_{4}$ with respect to the base frame {0} are expressed as:

$$ {}^{0}_{4}T = \begin{bmatrix} c_\alpha & s_\alpha s_\beta & c_\beta s_\alpha & r(c_\beta s_\alpha) \\ 0 & c_\beta & -s_\beta & r(-s_\beta) \\ -s_\alpha & c_\alpha s_\beta & c_\alpha & r(c_\alpha) \\ 0 & 0 & 0 & 1 \end{bmatrix} \tag{3.32} $$

$$ {}^{0}_{4}R = \begin{bmatrix} c_\alpha & s_\alpha s_\beta & c_\beta s_\alpha \\ 0 & c_\beta & -s_\beta \\ -s_\alpha & c_\alpha s_\beta & c_\alpha \end{bmatrix} \tag{3.33} $$

$$ {}^{0}P_{4x} = r(c_\beta s_\alpha) \tag{3.34} $$

$$ {}^{0}P_{4y} = r(-s_\beta) \tag{3.35} $$

$$ {}^{0}P_{4z} = r(c_\alpha) \tag{3.36} $$

In Introduction to Robotics, Craig book, the rotation matrix that 12 Euler angle sets is given;

$$ R_{XYZ'}(\alpha, \beta, \Upsilon) = \begin{bmatrix} c_\alpha c_\Upsilon + s_\alpha s_\beta s_\Upsilon & -c_\alpha s_\Upsilon + s_\alpha s_\beta c_\Upsilon & c_\beta s_\alpha \\ c_\beta s_\Upsilon & c_\beta c_\Upsilon & -s_\beta \\ -s_\alpha c_\Upsilon + c_\alpha s_\beta s_\Upsilon & s_\alpha s_\Upsilon + c_\alpha s_\beta c_\Upsilon & c_\alpha \end{bmatrix} \tag{3.37} $$

Where rotations performed about X by α, about Y by β, about Z by Υ and from the (3.33) and (3.37) matrices the following angles are obtained.

$$ \alpha = atan2(-R_{23}, R_{33}) \tag{3.38} $$

$$ \beta = atan2\left(R_{13}, \sqrt{{R_{11}}^2 + {R_{12}}^2}\right) \tag{3.39} $$

$$ \Upsilon = atan2(-R_{12}, R_{11}) \tag{3.40} $$

3.1.2. Inverse Kınematics

a) Inverse 1

Inverse kinematics is used to determine the joint positions that are required to achieve a desired end-effector orientation or position.

$$R_d = Rot_x(\phi)Rot_y(\Psi)Rot_z(\vartheta) \tag{3.41}$$

Where R_d is the desired rotation matrix and equal to (3.37).

$$R_d = \begin{bmatrix} R_{11} & R_{12} & R_{13} \\ R_{21} & R_{22} & R_{23} \\ R_{31} & R_{32} & R_{33} \end{bmatrix} \tag{3.42}$$

$$\alpha = atan2\left(-R_{31}, \sqrt{{R_{32}}^2 + {R_{33}}^2}\right) \tag{3.43}$$

$$\beta = atan2(R_{13}, R_{33}) \tag{3.44}$$

$$\Upsilon = atan2(R_{21}, R_{11}) \tag{3.45}$$

b) Inverse 2

In this section the values of $\hat{n}_P$ and r are computed as a function in terms of α, β and Υ. It was calculated in the Forward 2 section of $\hat{n}_P$ and it was also shown how it was calculated.

$$\hat{n}_P = \begin{bmatrix} c_\alpha c_\beta \\ s_\alpha s_\beta \\ -s_\beta \end{bmatrix} \tag{3.46}$$

When (3.19), (3.22) and (3.23) are arranged and solved according to Δr from three equations, the following equation is obtained.

$$\Delta r = \frac{1}{2}\left(\sqrt{{l_2}^2 + (l_1 - r_0)^2 + (l_1 - r_0)\left(2(-l_1 + r_0)c_\varphi - A_1 + c_{2\varphi}(l_1 - r_0 + A_1)\right)} + l_1 - r_0 - A_1 - c_\varphi(l_1 - r_0 + A_1)\right) \quad (3.47)$$

Where $A_1 = \sqrt{\frac{{l_2}^2 - (l_1 - r)^2 s_\varphi}{\left(1 + c_\varphi\right)^2}}$

$$\Delta d = \frac{2\pi}{\Upsilon * p} \quad (3.48)$$

$$\Upsilon = \left[\frac{l_1 - l_3 - (1 + c_\varphi)\left(l_1 - \mathrm{r} + \sqrt{\frac{{l_2}^2 - (l_1 - r)^2 s_\varphi}{\left(1 + c_\varphi\right)^2}}\right)}{p}\right] * 2\pi \quad (3.49)$$

c) Inverse 3

In this section, an equation is derived based on $\hat{n}_P$ and r for link angle (θ_i). The vector x_i must be perpendicular to a unit vector $\hat{u}$.

$$x_i \hat{u} = 0 \quad (3.50)$$

and vector ${}^B M_i$ is defined as follows in the (3.5).

$$\frac{P}{2}\hat{u} + x_i = {}^B M_i \quad (3.51)$$

$$\left({}^{B}M_i - \frac{P}{2}\hat{u}\right)\hat{u} = 0 \tag{3.52}$$

$$\hat{u} = \frac{{}^{B}P}{|{}^{B}P|} \tag{3.53}$$

$${}^{B}P = r(\hat{n}_B + \hat{n}_P) \tag{3.54}$$

Where $\hat{n}_B = [1 \quad 0 \quad 0]^T$ and $\hat{n}_P = [\hat{n}_{Px} \quad \hat{n}_{Py} \quad \hat{n}_{Pz}]^T$.

$$|{}^{B}P| = r\sqrt{(1+\hat{n}_{Px})^2 + \hat{n}_{Py}{}^2 + \hat{n}_{Pz}{}^2} \tag{3.55}$$

Substituting (3.5), (3.53) into (3.52), the constraint equation becomes for each serial link:

$$Fs_1(1+\hat{n}_{Px}) + \left(K_{1y} + Fc_1\right)\left(\hat{n}_{Py}\right) + \left(K_{1z} - \frac{\sqrt{3}F}{2}c_1\right)(\hat{n}_{Pz}) - r(1+\hat{n}_{Px}) = 0 \tag{3.56}$$

$$Fs_2(1+\hat{n}_{Px}) + \left(K_{2y} + Fc_2\right)\left(\hat{n}_{Py}\right) + \left(K_{2z} + \frac{\sqrt{3}F}{2}c_2\right)(\hat{n}_{Pz}) - r(1+\hat{n}_{Px}) = 0 \tag{3.57}$$

$$Fs_3(1+\hat{n}_{Px}) + \left(K_{3y}\right)\left(\hat{n}_{Py}\right) + (0)(\hat{n}_{Pz}) - r(1+\hat{n}_{Px}) = 0 \tag{3.58}$$

By substituting (3.1), (3.10), and (3.47) into (3.43), (3.44), (3.45) a set of 3 equations depending on θ_i for 3 identical legs composed of RSR joints,

$$X_i c_i + Y_i s_i + Z_i = 0 \tag{3.59}$$

Then, θ_i values can be computed by,

$$\theta_i = 2\tan^{-1}\left(\frac{Y_i \pm \sqrt{Y_i^2 + X_i^2 - Z_i^2}}{X_i - Z_i}\right) \tag{3.60}$$

3.2. Velocity Kinematic Analysis

Position kinematic analysis is used to generate velocity kinematic analysis of a robot,

$$v = J(q)\omega \tag{3.61}$$

where v is the output velocity vector and ω is the input velocity vector mapped into v by the Jacobian matrix J.

3.2.1. Jacobian Analysis

Time derivatives of forward kinematic equations can be used to find the mechanism's Jacobian matrix, which maps the link between actuator velocity and tool tip velocity.

The first step is to find the Jacobian matrix of the wrist part. With respect to link angles, tool unit vector of the top platform and thrust distance are differentiated.

$$J_w = \begin{bmatrix} \frac{\partial \hat{n}_{Py}}{\partial \theta_1} & \frac{\partial \hat{n}_{Py}}{\partial \theta_2} & \frac{\partial \hat{n}_{Py}}{\partial \theta_3} \\ \frac{\partial \hat{n}_{Pz}}{\partial \theta_1} & \frac{\partial \hat{n}_{Pz}}{\partial \theta_2} & \frac{\partial \hat{n}_{Pz}}{\partial \theta_3} \\ \frac{\partial r}{\partial \theta_1} & \frac{\partial r}{\partial \theta_2} & \frac{\partial r}{\partial \theta_3} \end{bmatrix} \tag{3.62}$$

The unit vector of the tool (3.13) is defined as a function of $\hat{u}$.

$$\frac{\partial \hat{n}_{Py}}{\partial \theta_i} = \frac{\partial (2\hat{u}_x \hat{u}_y)}{\partial \theta_i} \tag{3.63}$$

$$\frac{\partial \hat{n}_{Pz}}{\partial \theta_i} = \frac{\partial (2\hat{u}_x \hat{u}_z)}{\partial \theta_i} \tag{3.64}$$

$$\frac{\partial r}{\partial \theta_1} = \frac{1}{{u_x}^2} \frac{\partial (M_x u_x + M_y u_y + M_z u_z)}{\partial \theta_i} u_x - \frac{\partial (u_x)}{\partial \theta_i} (M_x u_x + M_y u_y + M_z u_z) \tag{3.65}$$

For the second step, J_T is determined by transforming the tool unit vector-thrust distance to the tool orientation angles-thrust distance.

$$J_T = \begin{bmatrix} & & 0 \\ & T_{2\times 2} & 0 \\ 0 & 0 & 1 \end{bmatrix} \tag{3.66}$$

Where $T_{2\times 2}$ makes it possible to transform $\{\hat{n}_{Py}, \hat{n}_{Pz}\}$ to $\{\alpha, \beta\}$.

$$T = \begin{bmatrix} \frac{1}{\sqrt{c^2\left(s^{-1}(-\hat{n}_{Pz})\right) - \hat{n}_{Py}{}^2}} & -\frac{s(s^{-1}(-\hat{n}_{Pz}))\hat{n}_{Py}}{c^2\left(s^{-1}(-\hat{n}_{Pz})\right)\sqrt{c^2\left(s^{-1}(-\hat{n}_{Pz})\right) - \hat{n}_{Py}{}^2}\sqrt{1-\hat{n}_{Pz}{}^2}} \\ 0 & -\frac{1}{\sqrt{1-\hat{n}_{Pz}{}^2}} \end{bmatrix} \quad (3.67)$$

For the third step, in up and down motion, the thrust distance and the linear displacement are both determined.

$$J_{\Delta d} = \begin{bmatrix} 1 & 0 & 0 \\ 0 & 1 & 0 \\ \frac{\partial \Delta d}{\partial \alpha} & \frac{\partial \Delta d}{\partial \beta} & \frac{\partial \Delta d}{\partial r} \end{bmatrix} \quad (3.68)$$

Finally, J_Υ is calculated using the linear displacement in up and down motion as well as the screw roll angle.

$$J_\Upsilon = \begin{bmatrix} 1 & 0 & 0 \\ 0 & 1 & 0 \\ 0 & 0 & \frac{\partial \Upsilon}{\partial \Delta d} \end{bmatrix} \quad (3.69)$$

It is shown in the following equation how to get from the motor velocities to wrist end effector velocities:

$$\begin{bmatrix} \dot{\alpha} \\ \dot{\beta} \\ \dot{r} \end{bmatrix} = J_T J_w \begin{bmatrix} \dot{\theta_1} \\ \dot{\theta_2} \\ \dot{\theta_3} \end{bmatrix} \quad (3.70)$$

The following step shows how to transform a change in thrust distance into a change in screw roll angle:

$$\begin{bmatrix} \dot{\alpha} \\ \dot{\beta} \\ \dot{\gamma} \end{bmatrix} = J_Y J_{\Delta d} \begin{bmatrix} \dot{\alpha} \\ \dot{\beta} \\ \dot{r} \end{bmatrix} \tag{3.71}$$

The total Jacobian of the 3 DOF system is the multiplication of (3.68), (3.67), (3.65), (3.61), and the Jacobian matrix is derived by directly differentiating the mechanism's kinematic equations.

$$J = J_Y J_{\Delta d} J_T J_w \tag{3.72}$$

4. WORKSPACE ANALYSIS

In robotic applications, it is very important to define the workspace clearly. The shortest and most reasonable way to achieve this clarity is to formulate. In this way, it can be learned whether the desired movements and configurations are possible. The workspace of a mechanism is revealed by defining all points reached by the mechanism in a 3-dimensional plot. The main reason for the limitation of movement in this mechanism and consequently the limitation of the workspace is the revolute motors. Working areas are restricted for revolute motors to move this mechanism without breaking it.

The limitations of the revolute motors are defined as,

$$\theta_{min} < \theta < \theta_{max} \tag{4.1}$$

Where θ_{min} and θ_{max} are the minimum and maximum degrees between bottom platform's front plane and leg modules which is attached to the motor. Parameters shown below in Figure 4.1.

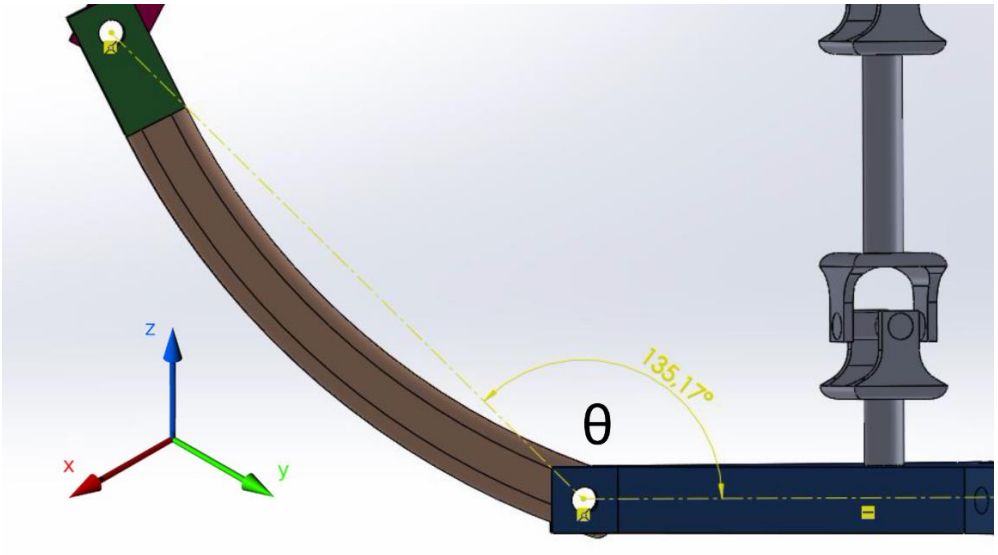

Figure 4.0.1. Revolute motors and θ angles locations

Each theta angle is independent of each other for the three leg modules. Although the intervals of the angles are fixed, it aims to reach the farthest points that can be reached by taking different angle values. To find the reachable boundary (workspace) in Cartesian space, advanced kinematic equations are applied "for loops" using MATLAB. The working space of the manipulator with the determination of the points reached by the end effector and shown in plot. In addition, when we examine Figure 4.2, the workspace is between ±125 mm in the x and y axes also between (-35) and 150 mm in the z axis.

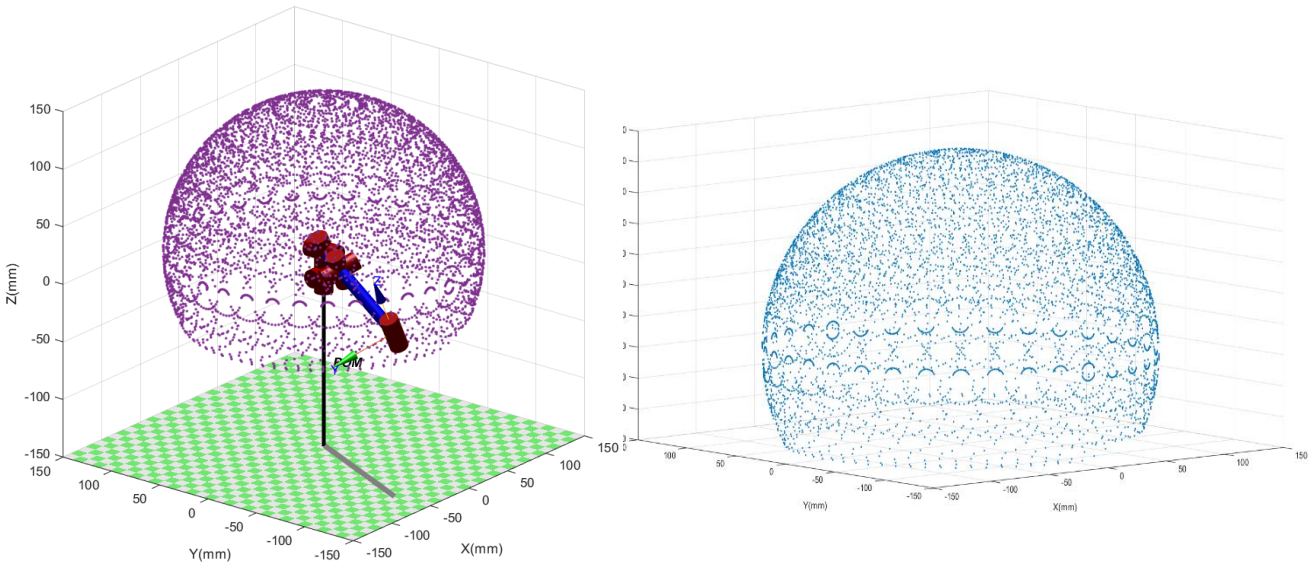

(a) (b)

Figure 4.0.2. The workspace of the 3 DOF Parallel Orientation Mechanism

In order to understand their appearance in more detail, an appropriate number of points (there are exactly 6385 points) were used in the MATLAB. Thus, a workspace that can be easily perceived even if there is a gap was created. You can see it in detail in Figures 4.3 and 4.4.

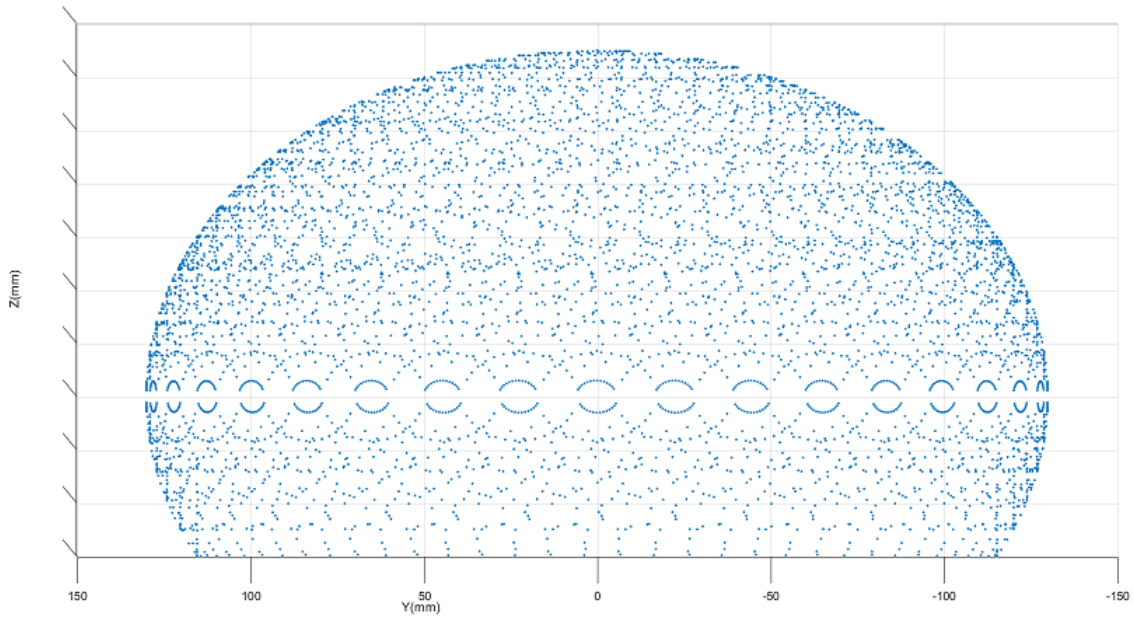

Figure 4.0.3. The workspace of the 3 DOF Parallel Orientation Mechanism about Y-Z Plane

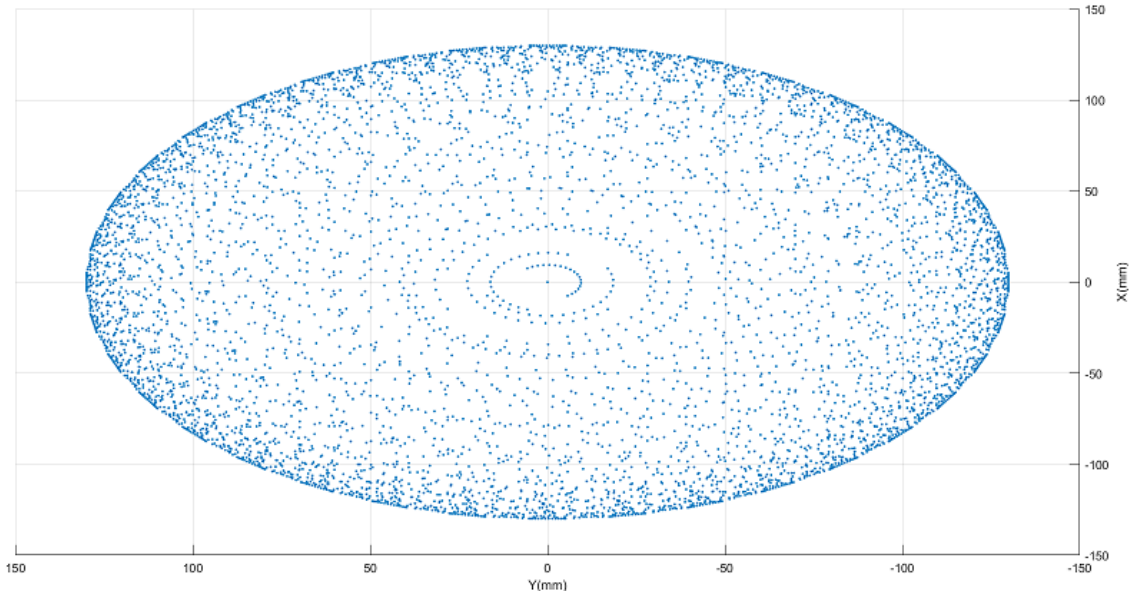

Figure 4.0.4. The workspace of the 3 DOF Parallel Orientation Mechanism about X-Y Plane

5.CONTROL SYSTEM OF MECHANISM

A proportional-integral-derivative (PID) controller is used to regulate the position of the 3 DOF mechanism, which is a common method. The wrist kinematic equations from Chapter 3 are used to create the control architecture.

5.1. PID Controller

PID (Proportional Integral Derivative) controllers are the most commonly utilized controllers in industrial settings because of its ease of use and the pleasure of performance they can provide the user for a wide range of processes. Despite the fact that the cost/benefit ratio given by these controllers is far superior than that of any other controller. Because of their widespread use, many strategies have been proposed for modifying the PID parameters, i.e. K_p, K_i, and K_d, as well as the installation of new capabilities that increase their performance. The block diagram of a simple PID controller is provided in the figure below.

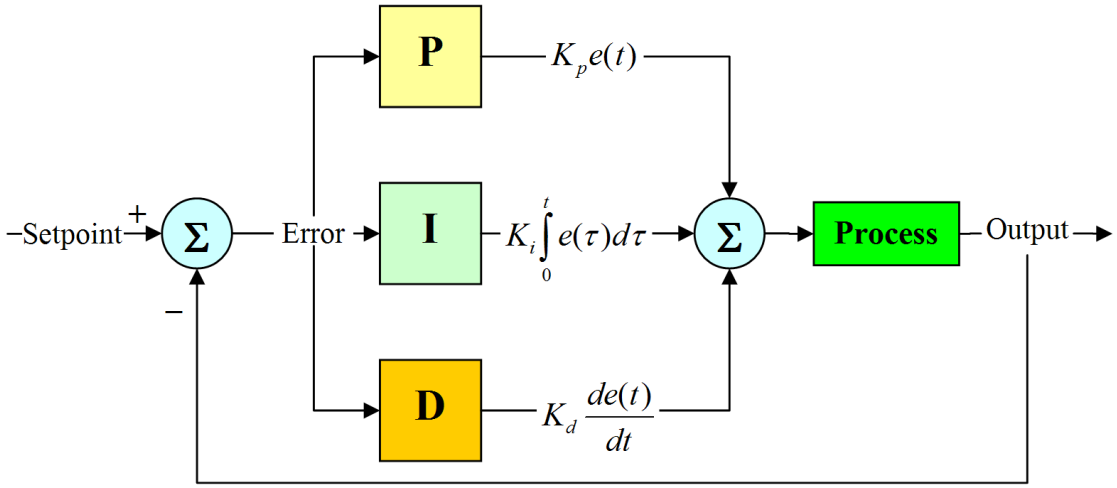

Figure 5.1. PID Block diagram

The output of a PID controller, which is equal to the control input to the plant, is calculated in the time domain from the feedback error as follows:

$$u(t) = K_p e(t) + K_i \int e(t)dt + K_d \frac{de}{dt} \tag{5.1}$$

where K_p = proportional gain, K_i = integral gain, and K_d = derivative gain.

The variable (e) represents the tracking error, the difference between the desired output (r) and the actual output (y). This error signal (e) is fed to the PID controller, and the controller computes both the derivative and the integral of this error signal with respect to time. The control signal (u) to the plant is equal to the proportional gain (K_p) times the magnitude of the error plus the integral gain (K_i) times the integral of the error plus the derivative gain (K_d) times the derivative of the error.

5.2. Dynamic Model of the Test System on Simulink

The next step in wrist mechanism design is to develop a control system. In this section, the orientation mechanism created in the CAD was transferred to the Simmechanics/MATLAB. Then, the control chart shown in the Figure 5.2 was created. Gravity is disabled. Then the configuration settings were made.

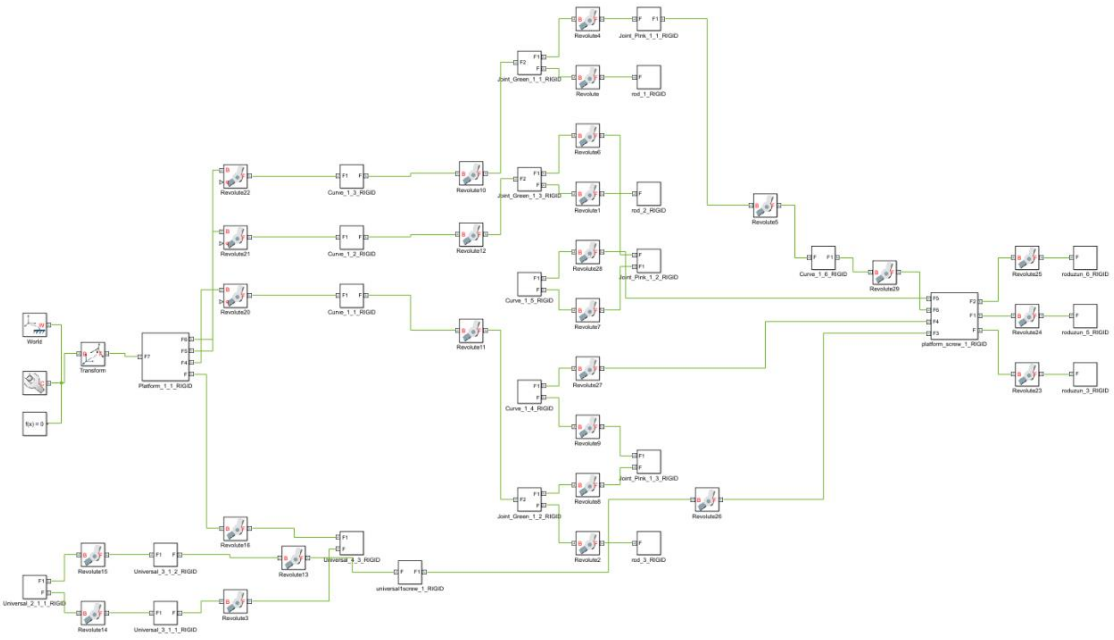

Figure 5.2. The mechanical model created using second generation in SimMechanics

Since the model transferred from CAD does not detect the screw joint, a lead screw joint has been added to the exported control scheme. It is shown in Figure 5.3. Screw joint parameters are entered according to the drawing.

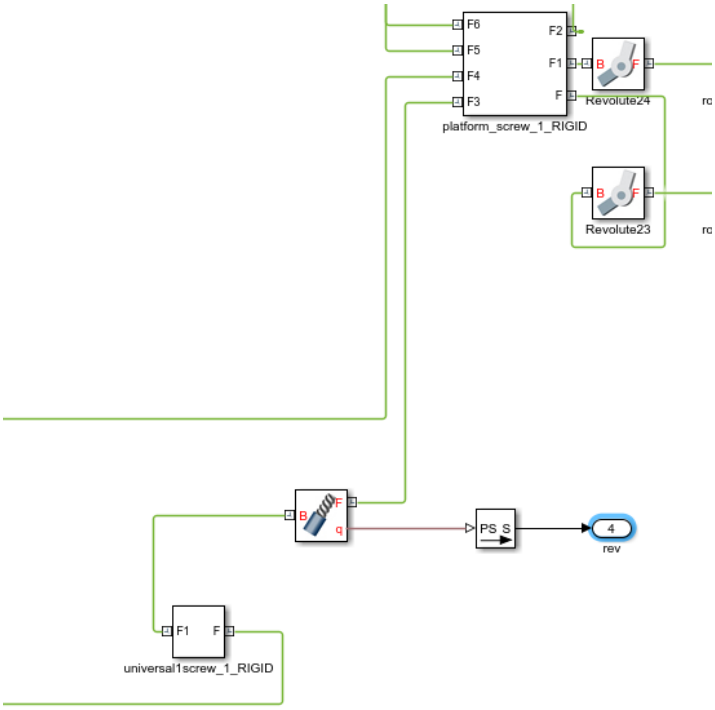

Figure 5.3. Lead screw joint

As indicated in Figure 5.4, α, β, and roll (in order to calculate the screw angle, the number of rotations is given as input) are given to the control system as reference inputs in these simulations. For joint-space control, inverse kinematic equations were used to transform pitch, yaw, and screw angles into motor position.

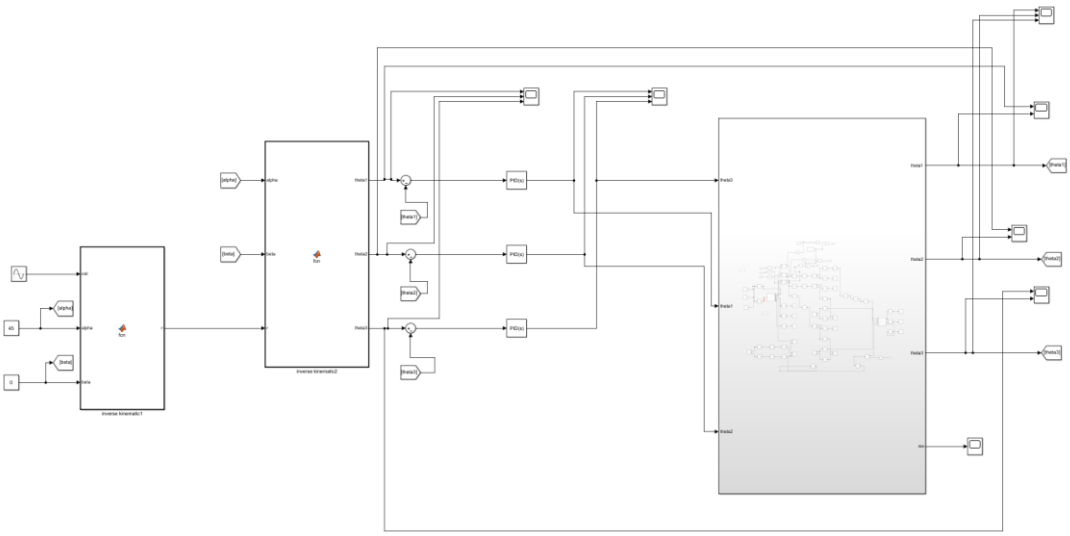

Figure 5.4 Simmechanics Model

The PID parameters used in this simulation are in the figure below.

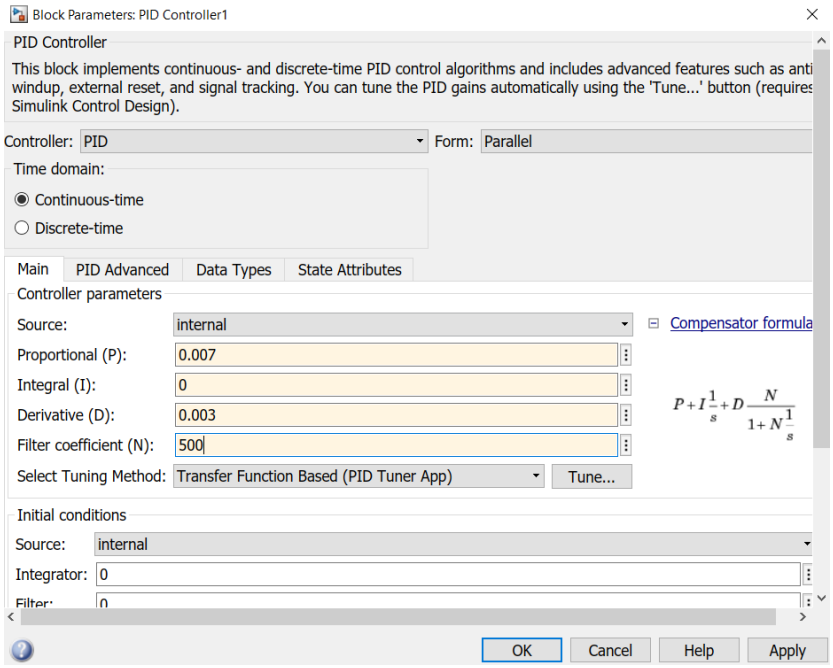

Figure 5.5. Block Parameters: PID Controller

Inverse kinematics, which can be found in the Inverse Kinematics section, was used on Simulink to get the tool to the appropriate position. The reference inputs α, β, and roll determine tool orientation. All details are in Appendix A.

Figure 5.6 shows the control input given to the system in the Simmechanics model, which is obtained from a mixture of PID controllers and gives desired motion based on the reference inputs.

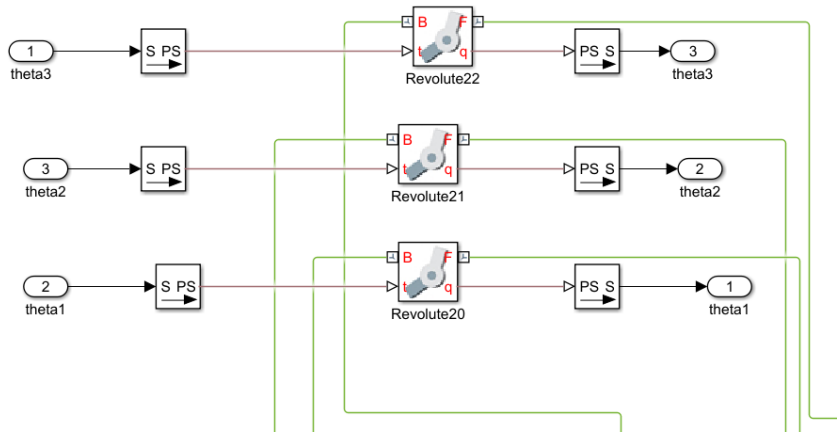

Figure 5.6. Inside the Subsystem

During the simulation, two different signal inputs, constant and sinusodial signal, were given. The given input values are sinusoidal signal for roll, 45 degrees for alpha and 0 degrees for beta.

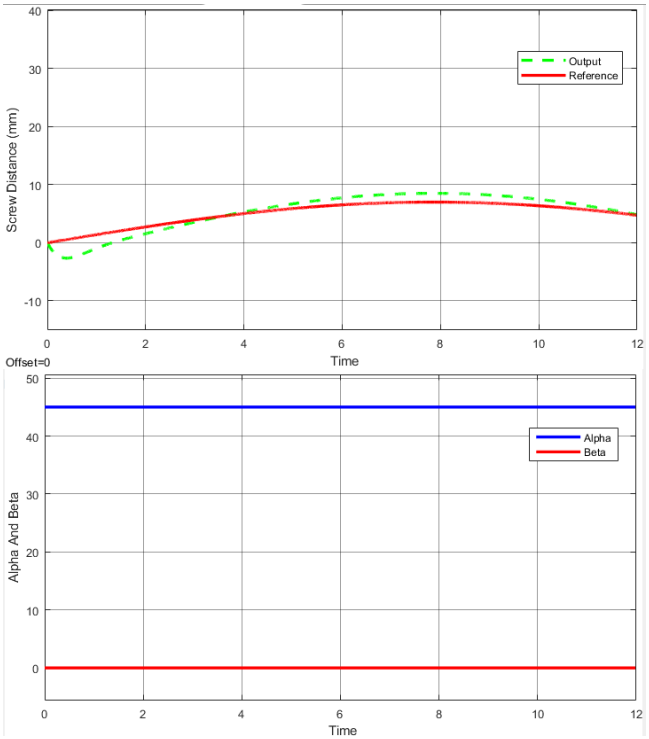

Figure 5.7 Input values, tool degrees

The sine wave parameters for the roll input are as in the figure below.

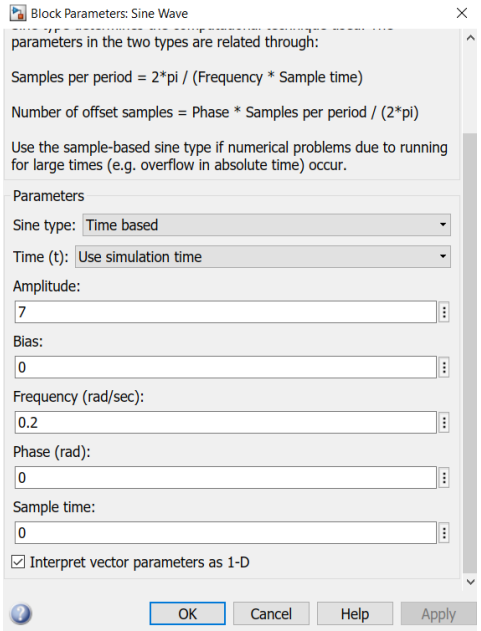

Figure 5.8. Sine Wave Parameters for Roll Input

As a result of these input values, the comparison of reference values and output values is shown in Figure 5.9. There are figures of values for θ_1, θ_2 and θ_3 from top to bottom.

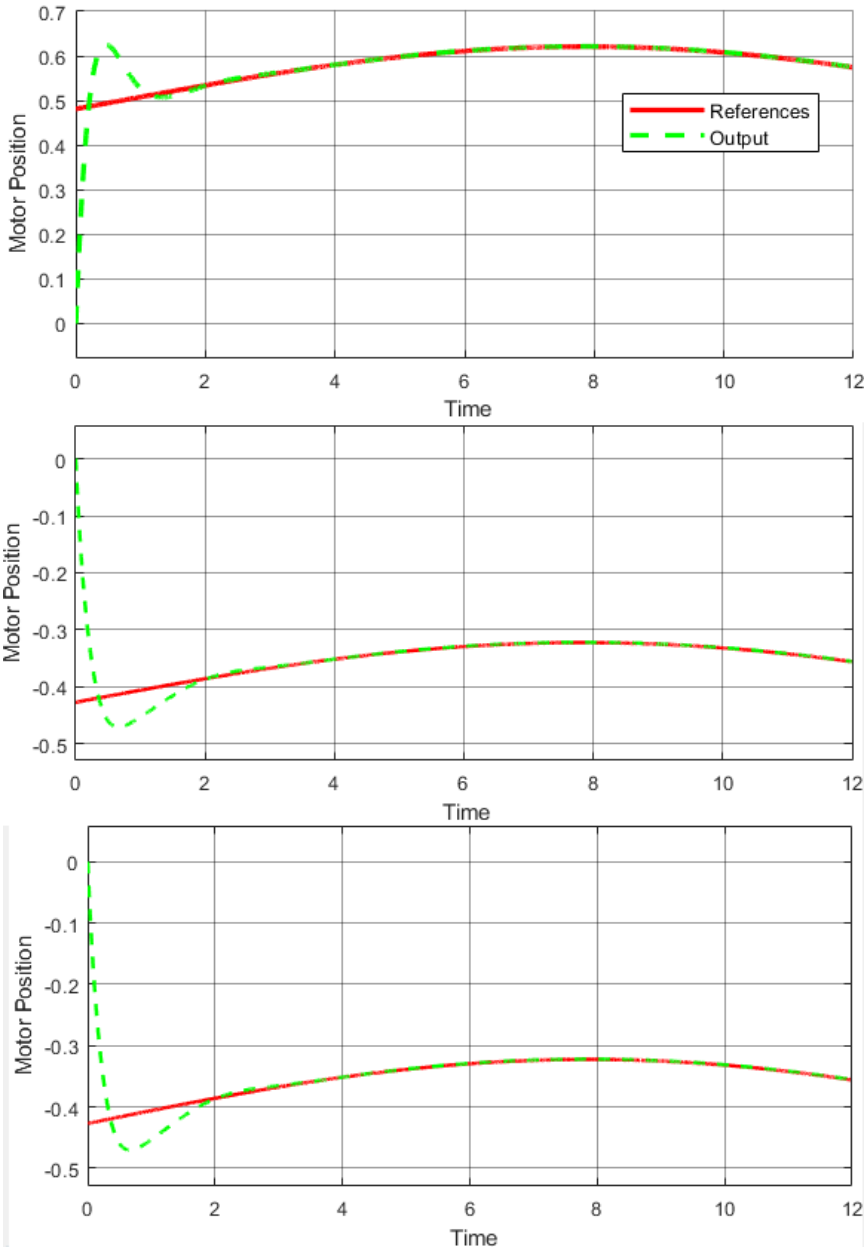

Figure 5.9. Results, θ_1, θ_2, θ_3

Although the output values differ from the reference values in the first 2 seconds, the desired values can be reached after 2 seconds. Although the movement of the screw and the movement of the mechanism, which is the aim here, are not provided in the first 2 seconds, they are provided for the later.

Secondly, when you give sinusoidal signal to the input of the alpha, 0 degrees to the beta and 3 to the roll movement, the results are as in the figure below.

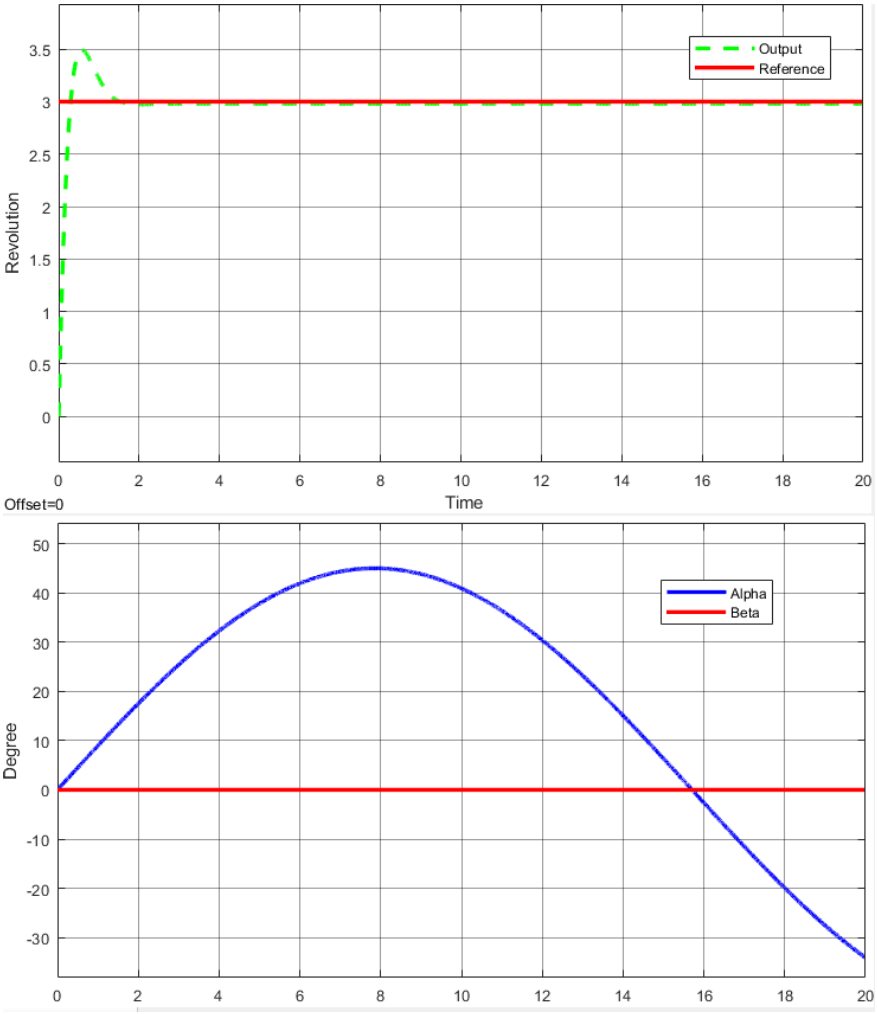

Figure 5.10 Input values, Tool degrees

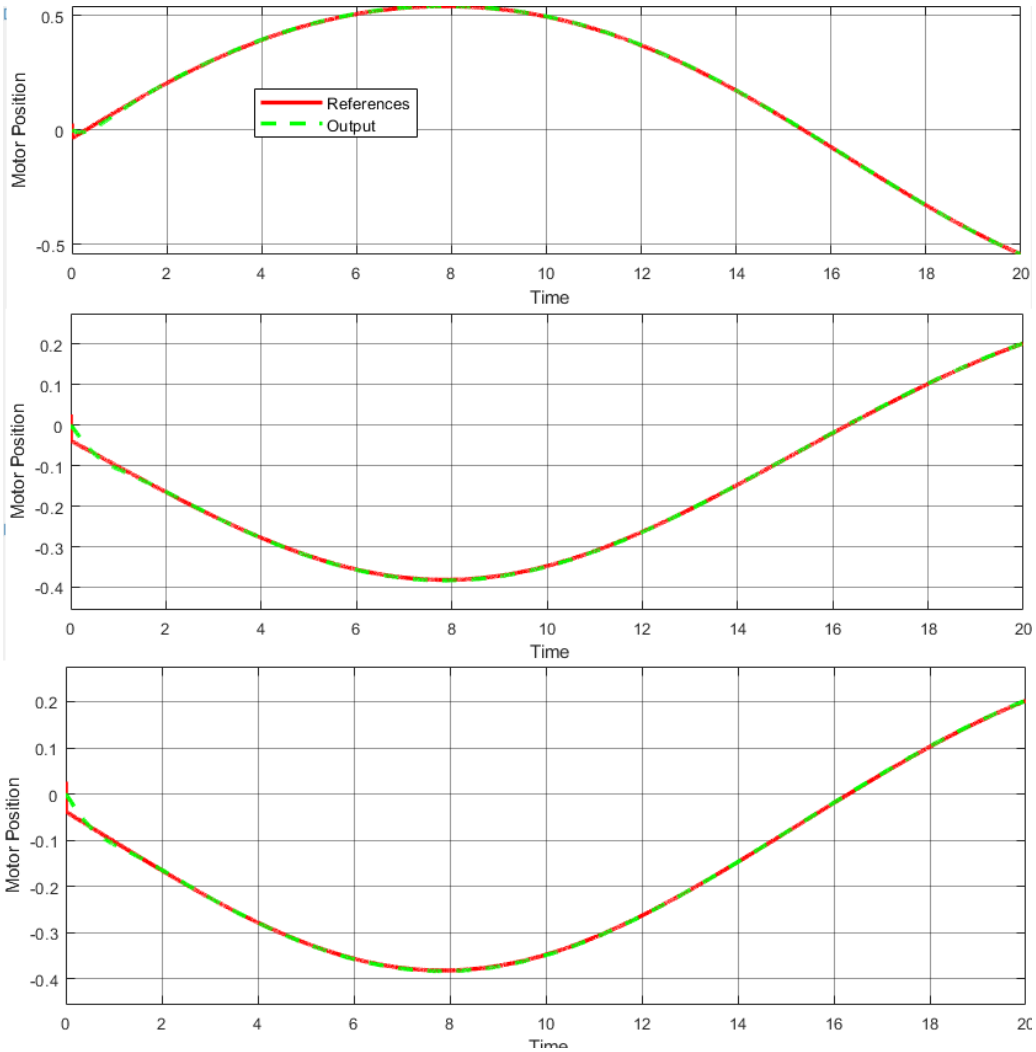

Figure 5.11. Results, θ_1, θ_2, θ_3

When we look at Figure 5.11, we see that the kinematic equations and the control system work correctly. The red line, which is the reference line, and the green dotted line, which is the engine outout line, coincide. While the graphs of θ_2 and θ_3 are the same, the graph of θ_1 is different because the other arm is doing the same movement while the other arm is doing the opposite.

The maximum value we can give without having a singularity problem or a screw problem in the established control system is alpha 60 degrees, beta 0 degrees. The graph of the input values is given in Figure 5.12.

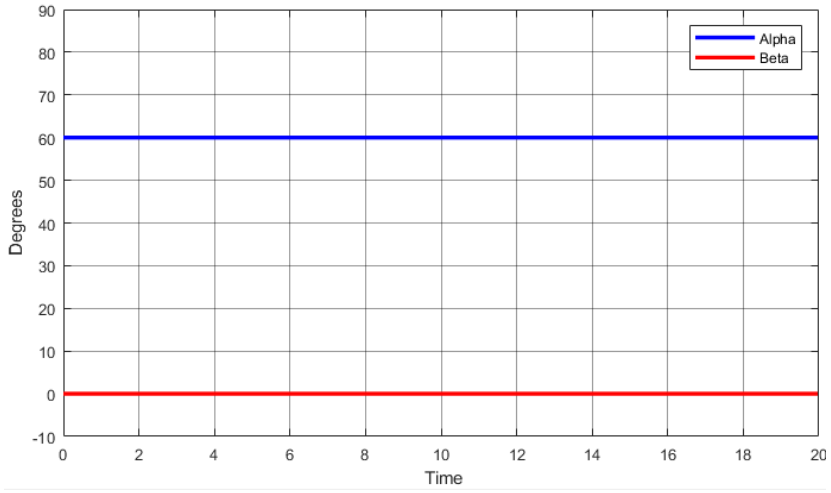

Figure 5.12 Input values

In Figure 5.13, there is a graph of the result values. The first graph is θ_1 motor output and the second is screw displacement output. While the control is achieved successfully in the motor outputs, there is a small margin of error in the screw joint.

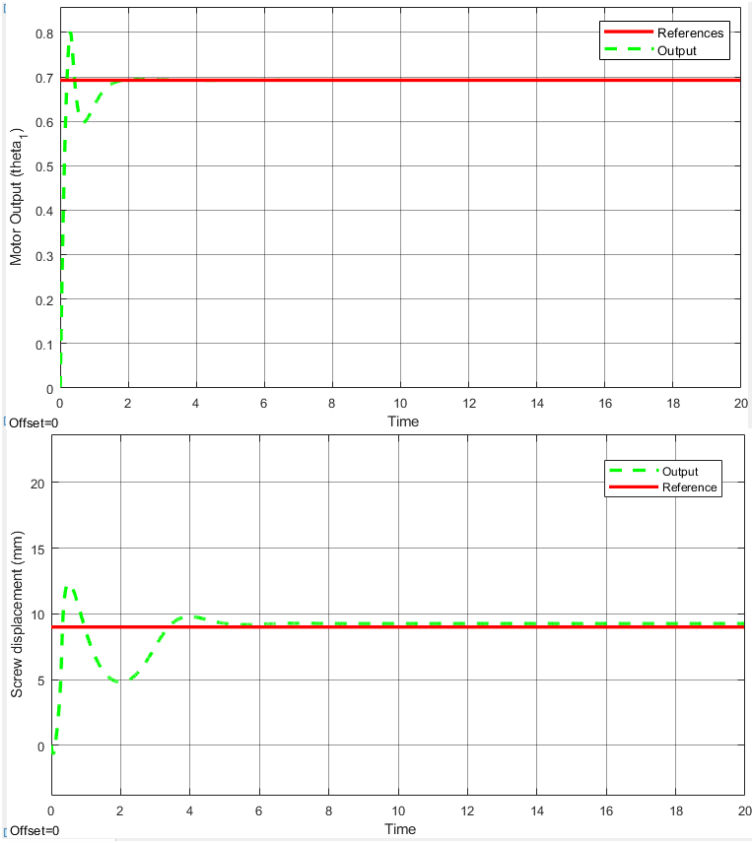

Figure 5.13 Output values

In the figure below, there is the image obtained in the simulation. The angle between the two arms and the bottom platform is approximately 180 degrees. The most bending obtained by giving the alpha value 60 degrees is as in the figure. In further bending, control cannot be achieved. It gives a screw joint error.

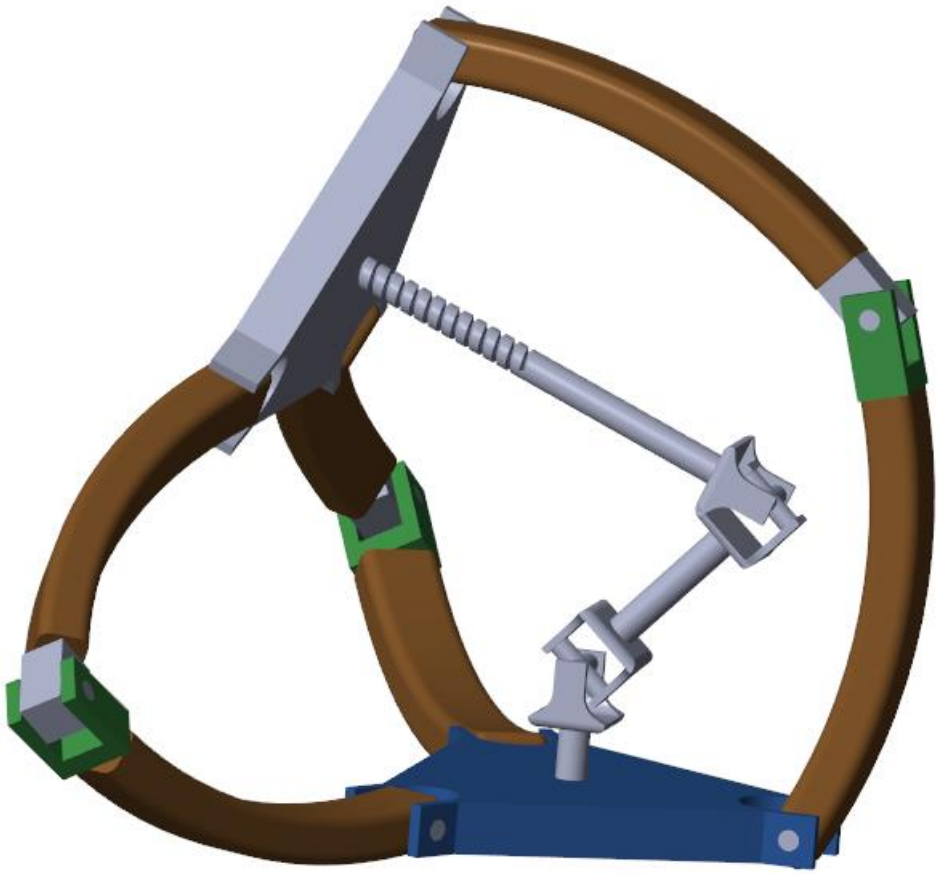

Figure 5.14 Figure of simulation

Figure 5.15 shows the most bending obtained in SolidWorks environment. The angle between the arm and the bottom platform reaches a maximum of 208 degrees. This gives us ±208 degrees of range of motion. In more cases, the singularity problem is encountered and the shape is distorted.

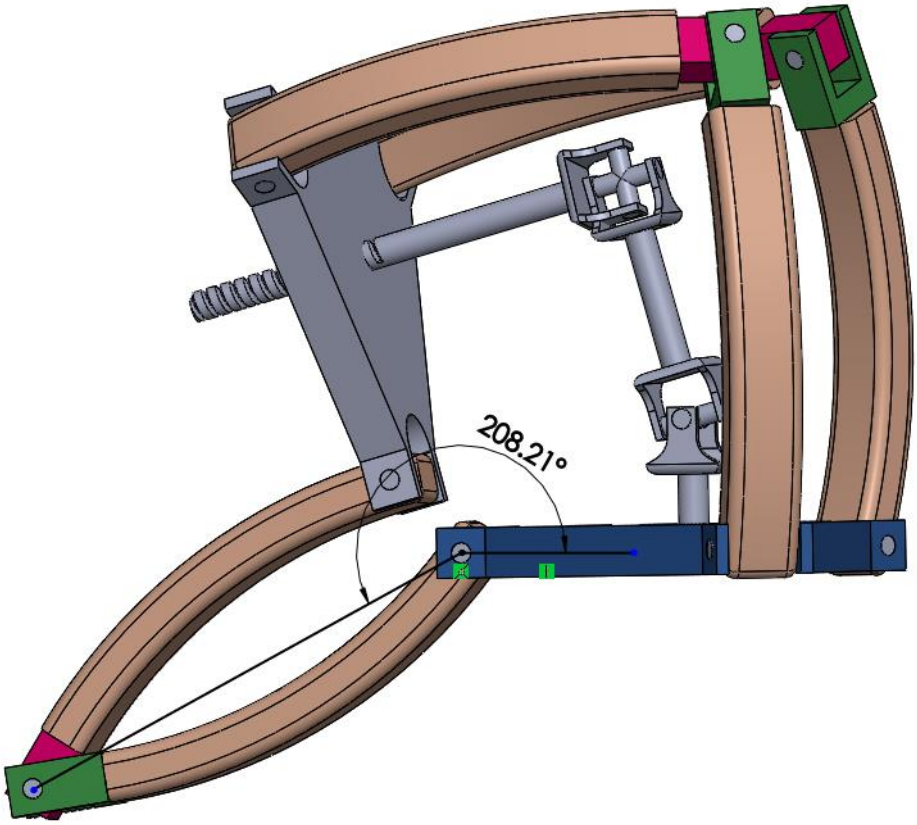

Figure 5.15 Figure of SolidWorks

6. CONCLUSIONS

This thesis presents a new design of the 3 DOF parallel orientation mechanism, which is more economical and provides more movement space. This mechanism provides movement in ±120 degrees pitch and yaw axes, and on the axis of rotation, it can rotate ±360 degrees thanks to the screw on the upper platform. It can do all these movements with only 3 rotation motors. All these requests have been produced as a solution to the open-ended problem.

In line with these requests, 2 different designs were made and the most suitable one among these designs was selected and continued with that design. Since the second design provides the movements I want in the Solidworks environment without getting stuck with the singularity problem, the kinematic analysis of the second design has been started.

In order to analyze the mechanism, a mathematical model was created by deriving the forward and inverse equations. In addition, velocity kinematic analysis was used to derive the Jacobian matrix. The workspace analysis of only 3 arms was made without the screw joint and the universal joint in the middle, using position kinematics. Workspace analysis of the entire mechanism could not be performed.

In order to control the position of the mechanism, PID controller is applied in the simulation model. Certain angles and rotations are given, mechanism and kinematic equations are tested, and 2 results are added to the thesis. As a result of the experiment, kinematic equations (inverse kinematics) were verified in Simmechanics. The kinematic equations and simulation motion were compared with the PID controller. When the figures were examined, it was observed that the robot generally followed the reference signals correctly.

As a result, although it is observed in the control part that the screw joint sometimes does not move as desired in the first place, it generally provides the desired angle in the desired pitch and yaw axis and does not get into the singularity problem. The problem can be improved by a detailed research on screw joint use in Simmechanics or by using a different screw design turning design.

REFERENCES

1. MERLET, Jean-Pierre; GOSSELIN, Clément. Parallel Mechanisms and Robots. 2008.

2. PATEL, Y. D., et al. Parallel manipulators applications—a survey. Modern Mechanical Engineering, 2012, 2.03: 57.

3. CHAPARRO-ALTAMIRANO, Daniel; ZAVALA-YOE, Ricardo; RAMÍREZ-MENDOZA, Ricardo. Kinematic and workspace analysis of a parallel robot used in security applications. In: 2013 International Conference on Mechatronics, Electronics and Automotive Engineering. IEEE.

4. TAGHIRAD, Hamid D. Parallel robots: mechanics and control. CRC press, 2013.

5. MERLET, Jean-Pierre. Parallel robots. Springer Science & Business Media, 2005. pages 5-11.

6. KAROUIA, Mourad; HERVÉ, Jacques M. An orientational 3-dof parallel mechanism. In: Proceedings of the 3rd Chemnitz Parallel Kinematics Seminar. Chemnitz, Germany, April, 2002. p. 139-150.

7. DASGUPTA, Bhaskar; MRUTHYUNJAYA, T. S. Singularity-free path planning for the Stewart platform manipulator. Mechanism and Machine Theory, 1998, 33.6: 711-725.

8. LIU, Kai; FITZGERALD, John M.; LEWIS, Frank L. Kinematic analysis of a Stewart platform manipulator. IEEE Transactions on industrial electronics, 1993, 40.2: 282-293.

9. REY, L.; CLAVEL, R. The delta parallel robot. In: Parallel Kinematic Machines. Springer, London, 1999. p. 401-417.

10. UZUNOVIC, Tarik, et al. Configuration space control of a parallel Delta robot with a neural network based inverse kinematics. In: 2013 8th International Conference on Electrical and Electronics Engineering (ELECO). IEEE, 2013. p. 497-501.

11. HOSSEINI, Mir Amin; DANIALI, Hamid-Reza Mohammadi. Kinematic analysis of tricept parallel manipulator. IIUM Engineering Journal, 2011, 12.5.

12. SICILIANO, Bruno. The Tricept robot: Inverse kinematics, manipulability analysis and closed-loop direct kinematics algorithm. Robotica, 1999, 17.4: 437-445.

13. CHAPARRO-ALTAMIRANO, Daniel; ZAVALA-YOE, Ricardo; RAMIREZ-MENDOZA, Ricardo. Dynamics and control of a 3SPS-1S parallel robot used in security applications. In: 21st International Symposium on Mathematical Theory of Networks and Systems, MTNS, Groningen, T.

14. ZAVALA-YOÉ, Ricardo; RAMÍREZ-MENDOZA, Ricardo A.; CHAPARRO-ALTAMIRANO, Daniel. Kinematic and Dynamical Modelling for Control of a Parallel Robot-based Surveillance/Sentry Device. Advances in Military Technology, 2015, 10.1.

15. KAZEZKHAN, Guljaina, et al. Dynamic modeling of the Stewart platform for the NanShan Radio Telescope. Advances in Mechanical Engineering, 2020, 12.7: 1687814020940072.

16. GOSSELIN, Clément M.; HAMEL, J.-F. The agile eye: a high-performance three-degree-of-freedom camera-orienting device. In: Proceedings of the 1994 IEEE international conference on robotics and automation. IEEE, 1994. p. 781-786.

17. BONEV, Ilian A.; CHABLAT, Damien; WENGER, Philippe. Working and assembly modes of the Agile Eye. In: Proceedings 2006 IEEE International Conference on Robotics and Automation, 2006. ICRA 2006. IEEE, 2006. p. 2317-2322.

18. ROSHEIM, Mark E.; SAUTER, Gerald F. New high-angulation omnidirectional sensor mount. In: Free-Space Laser Communication and Laser Imaging II. International Society for Optics and Photonics, 2002. p. 163-174.

19. SOFKA, J., et al. Omni-Wrist III-a new generation of pointing devices. Part I. Laser beam steering devices-mathematical modeling. IEEE transactions on aerospace and electronic systems, 2006, 42.2: 718-725.

20. ITUL, T.; PISLA, D. Dynamics of a 3-DOF parallel mechanism used for orientation applications. In: 2008 IEEE International Conference on Automation, Quality and Testing, Robotics. IEEE, 2008. p. 398-403.

21. BAJAJ, Neil M.; DOLLAR, Aaron M. Kinematic Optimization of a Novel Partially Decoupled Three Degree of Freedom Hybrid Wrist Mechanism. In: 2018 IEEE International Conference on Robotics and Automation (ICRA). IEEE, 2018. p. 6953-6960.

22. M. Bazman, N. Yilmaz, and U. Tumerdem, “Dexterous and back-drivable parallelrobotic forceps wrist for robotic surgery,” Proc. - 2018 IEEE 15th Int. Work. Adv.Motion Control. AMC 2018, pp. 153–159, 2018.

23. N. Yilmaz, M. Bazman, and U. Tumerdem, “External Force/Torque Estimation on a Dexterous Parallel Robotic Surgical Instrument Wrist,” 2018 IEEE/RSJ Int. Conf. Intell. Robot. Syst., pp. 4396–4403, 2019.

24. A. Alassi, N. Yilmaz, M. Bazman, B. Gur, and U. Tumerdem, “Development and kinematic analysis of a redundant, modular and backdrivable laparoscopic surgery robot,” IEEE/ASME Int. Conf. Adv. Intell. Mechatronics, AIM, vol. 2018-July, pp. 213–219, 2018.

25. Majid, M. Z. A., Huang, Z., & Yao, Y. L. (2000). Workspace analysis of a six-degrees of freedom, three-prismatic-prismatic-spheric-revolute parallel manipulator. The International Journal of Advanced Manufacturing Technology, 16(6), 441-449.

APPENDIX A

Details of Blocks in Control System

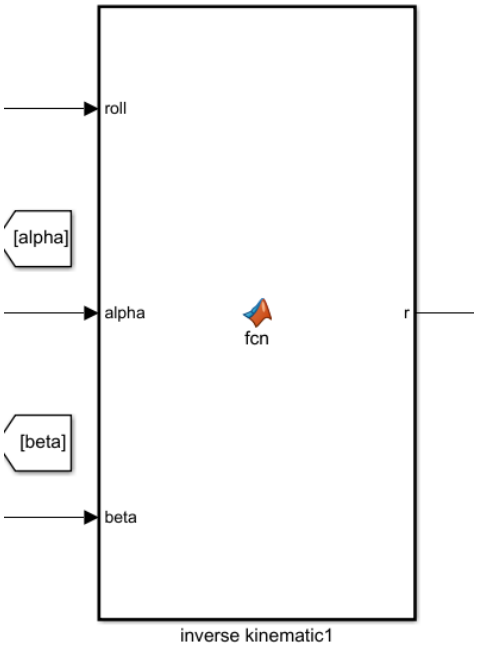

Matlab Code of Inverse Kinematic1 Block

```
function r  = fcn(roll,alpha,beta)

dg= roll*3;
r0=70;
v=0;

l1=24.24;
l2=45.61;
l3=61.12;

alpha=alpha*pi/180;
beta=beta*pi/180;
n=[cos(alpha)*cos(beta);sin(alpha)*cos(beta);-sin(beta)];
ndik=[1;0;0];
phi=acos(dot(ndik,n)/(norm(ndik)*norm(n)));
```

```
Tw=[cos(alpha)*cos(beta) -sin(alpha) cos(alpha)*sin(beta)
r0*(1+cos(alpha)*cos(beta));
    sin(alpha)*cos(beta) cos(alpha) sin(alpha)*sin(beta)
r0*sin(alpha)*cos(beta);
    -sin(beta) 0 cos(beta) -r0*sin(beta);
    0 0 0 1] ;
x=Tw(1,4);
y=Tw(2,4);
z=Tw(3,4);
rd_phi=0;

if alpha==0 && beta==0
    rd_phi=dg/2;
    r=r0+rd_phi;
else
    rd_phi= dg/2 + l1/2 + l2/2 + l3/2 - r0 - ((l2 -
(l2^2*tan(phi/2)^2 - l1^2*tan(phi/2)^2 - dg^2*tan(phi/2)^2 -
l3^2*tan(phi/2)^2 + l2^2 + 2*dg*l1*tan(phi/2)^2 -
2*dg*l3*tan(phi/2)^2 +
2*l1*l3*tan(phi/2)^2)^(1/2))*((l2*tan(phi/2))/2 -
(l1*tan(phi/2))/2 + (l3*tan(phi/2))/2 +
(dg*tan(phi/2))/2))/(l2*tan(phi/2) - l1*tan(phi/2) +
l3*tan(phi/2) + dg*tan(phi/2));



    r=r0+rd_phi;
end
```

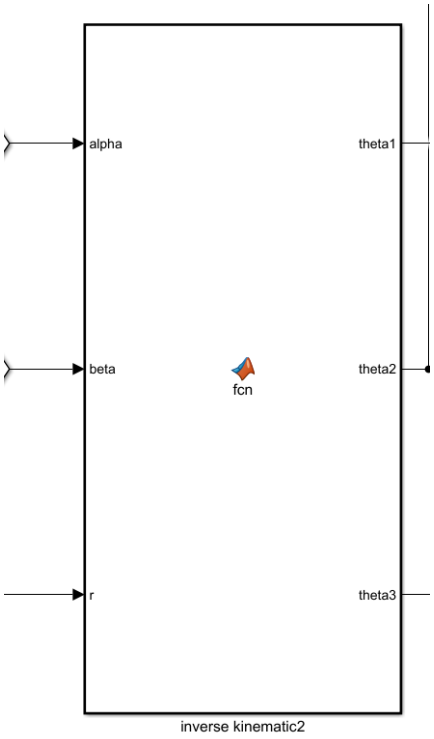

Matlab Code of Inverse Kinematic2 Block

```
function [theta1,theta2,theta3] = fcn(alpha,beta,r)
a1=alpha*pi/180;
b1=beta*pi/180;
nx=cos(a1)*cos(b1);
ny=sin(a1)*cos(b1);
nz=-sin(b1);
N=100.37; %%mm
Lo=157.321; %%mm
% r=140.716/2; %%mm
%% Coefficient of Equation1
X1=N*ny;
Y1=N*(1+nx);
Z1=(-r*(1+nx)-Lo*ny/(2*sqrt(3)));
%% Coefficient of Equation2
X2=-N/2*(ny-sqrt(3)*nz);
Y2=Y1;
Z2=(-r*(1+nx)+Lo/4*(1/sqrt(3)*ny-nz));
%% Coefficient of Equation3
X3=-N/2*(ny+sqrt(3)*nz);
```

```
Y3=Y1;
Z3=(-r*(1+nx)+Lo/4*(1/sqrt(3)*ny+nz));

t0 = 133.61*pi/180;
theta1=-2*atan(((-Y1-sqrt(X1^2+Y1^2-Z1^2))/(Z1-X1))) + t0;
theta2=-2*atan(((-Y2-sqrt(X2^2+Y2^2-Z2^2))/(Z2-X2))) + t0;
theta3=-2*atan(((-Y3-sqrt(X3^2+Y3^2-Z3^2))/(Z3-X3))) + t0;

end
```